Remote Sensing Applications: Society and Environment 39 (2025) 101690

Contents lists available at ScienceDirect

Remote Sensing Applications: Society and Environment

journal homepage: www.elsevier.com/locate/rsase

Potential of sentinel 2-derived canopy water content as an indicator of flash drought: Case studies from European cereal crop areas

Zaib Unnisa *, Booker Ogutu, Jadunandan Dash

School of Geography and Environmental Science, University of Southampton, SO17 1BJ, United Kingdom

ARTICLE INFO

Keywords:
Canopy water content
Drought indicator
Flash drought
Crop stress
Sentinel 2 level 2 processor
Biophysical variables
Evaporative stress index

ABSTRACT

Flash droughts are concerning due to their rapid onset and intensification by heatwaves and rainfall deficit. This leads to rapid soil moisture depletion, causing crops to desiccate and die faster than in slow droughts, especially during critical crop growth stages, which affects the yield. The early detection of flash droughts is possible through the evaluation of the response of plant biophysical variables to these events. To assess that, this study analysed three crop biophysical variables and vegetation index derived from Sentinel-2 across distinct cereal-growing regions in Europe (ROI-1: Southern Spain; ROI-2: Northern Italy; ROI-3: Eastern Hungary) to evaluate their potential for detecting flash droughts. The Evaporative Stress Index (ESI) was used for detecting the drought onset, intensity, and duration, and the response of Normalized Difference Vegetation Index (NDVI), Leaf Area Index (LAI), Fraction of Absorbed Photosynthetically Active Radiation (fAPAR), and Canopy Water Content (CWC) were compared using spatio-temporal comparison and Pearson correlation for Wheat and Maize crops in Summer 2022 and Spring 2023 droughts. The findings revealed that CWC showed the earliest response to flash drought over irrigated areas of Spain and Italy compared to LAI and fAPAR. During drought, strong correlations between CWC and ESI (wheat and maize) (in ROI 1, $r = 0.59$ and ROI 2, $r = 0.66$) reflected a higher degree of conformity in capturing drought. However, the sensitivity of CWC to flash drought varied in the rainfed region, with weaker correlation observed in Eastern Hungary, where $r = 0.4$, ROI 3. These results show that there is potential in Sentinel 2-based CWC for early detection of flash droughts, particularly in irrigated systems. It can provide reliable and traceable information about crop stress at the onset of flash drought.

1. Introduction

Flash droughts are rapid-onset, short-term drought events characterized by a swift decline in soil moisture and precipitation deficits, typically developing over a few weeks. They often intensify heat and water stress on vegetation and crops much faster than traditional droughts. Flash droughts can occur as isolated events or as sudden intensifications of existing drought conditions and, if not alleviated by rainfall, have the potential to transition into longer-lasting drought episodes (Hari et al., 2020; Markonis et al., 2021). Their frequent occurrences have caused collective damage to the agriculture, energy, and water sectors, with approximately €9 billion

* Corresponding author.
E-mail address: z.un-nisa@soton.ac.uk (Z. Unnisa).

https://doi.org/10.1016/j.rsase.2025.101690
Received 3 March 2025; Received in revised form 16 June 2025; Accepted 12 August 2025
Available online 13 August 2025

loss in Europe, in which agriculture bears the largest share, 50 % (Cammalleri et al., 2022; Naumann et al., 2021).

Since 2018, Europe has experienced persistent sub-seasonal-to-seasonal flash droughts, which are considered an unprecedented climatic phenomenon in the region over the past 250 years. These droughts are closely linked to Europe's unique climatic and geographic conditions, including its temperate climate zones and complex land-sea interactions. They are not isolated events but rather symptomatic of a larger, evolving pattern driven by extreme temperature anomalies (+2.8 °C) and precipitation deficits. The seasonal rainfall patterns in Europe are influenced by the Atlantic Ocean and Mediterranean weather systems, which can create irregular and sometimes sharply reduced precipitation events, intensifying dry spells. European landscapes, dominated by a mix of agriculture, forests, and heterogeneous soils, affect moisture cycling. Dry soils and stressed vegetation reduce evapotranspiration by about 50 %, which can suppress local rainfall and exacerbate drought conditions (Hansel et al., 2022). The 2022 drought exemplified this trend, with persistent rainfall deficits combined with heat waves in May, June, and July, worsening soil moisture shortages, and causing further drought expansion. These conditions are strongly influenced by Europe's regional climatic dynamics, such as rising temperatures and altered atmospheric circulation patterns, amplified extreme weather events, making flash droughts more frequent and severe. It severely impacted crop health, particularly in key agricultural regions, including northern Italy, southern and central France, central Germany, eastern Hungary, Portugal, and Spain (Hari et al., 2020; Markonis et al., 2021; Hansel et al., 2022). The summer 2022 and spring 2023 episodes were one of Europe's deadliest droughts on record, resulting in a staggering potential revenue loss of €25–30 billion for farming, affecting approximately half of the region, in which maize and wheat crops were notably affected. These agricultural losses were disproportionately concentrated in the Western Mediterranean and Carpathian-Balkan parts of Europe, pointing out that some areas in Europe are more susceptible to droughts than others (Pinke et al., 2024). With increased evaporation and decreased rainfall, there will be more frequent and severe droughts, particularly in the Mediterranean and Atlantic regions of Europe (Rakovec et al., 2022). This risk of occurrence is predicted to escalate in Europe (from 32 % to 53 %) under the most extreme emissions scenario between 2015 and 2100 (Christian et al., 2023). Effective monitoring of these events is crucial to enable timely mitigation strategies and reduce substantial agricultural and economic losses.

Early forecasting of flash droughts is critical but remains difficult due to the rapid development of these events and the complex interplay of climatic, vegetation, and hydrological factors that govern their onset and progression. Traditional drought indices such as the Palmer Drought Severity Index (PDSI- Palmer, 1965), Standardized Precipitation Evapotranspiration Index (SPEI – Vicente Serrano et al., 2010), and Standardized Precipitation Index (SPI- Guttman, 1998; Zargar et al. 2011), are not sufficient alone, though they provide insight into moisture deficits leading to drought onset; but they treat plants as static entities and do not accurately represent soil moisture available for plant growth (Yihdego et al., 2019; Chang et al., 2023). Based on available soil moisture, vegetation responds rapidly to soil moisture decline along its cycle, initiates metabolic and morphological defense mechanisms, and reduces photosynthetic activity when drought occurs. These immediate physiological responses make vegetation-based remote sensing (RS) indicators special for early flash drought detection. Because of that, 90 % of studies on flash droughts rely on high-resolution RS-based indicators, while only 10 % use traditional indices for monitoring hydrological and meteorological droughts (Alahacoon and Edirisinghe, 2022).

On the other hand, conventional vegetation indices such as NDVI and vegetation condition index (VCI) have limitations in detecting flash droughts. While they effectively monitor regular, slow-developing droughts by tracking vegetation and moisture changes over time and show strong negative correlations between LST and VCI ($r = -0.71$) and NDVI ($r -0.73$) reflect how negatively higher temperatures affect the health of the vegetation, which in turn increases the sensitivity to drought (Burka et al., 2024). NDVI often struggles to detect quick reductions in plant activity, especially when structural vegetation changes are subtle or absent, and it frequently saturates the signal in dense canopies where Leaf Area Index (LAI) is typically high, limiting its sensitivity to early physiological stress (Gao et al., 2023). VCI, derived from NDVI anomalies, reflects vegetation stress over time but similarly lags in identifying fast-onset moisture deficits. In comparison, the weekly Standardized Vegetation Index (SVI) better captures these rapid changes (Dutta et al., 2015). Similarly, Vegetation Health Index (VHI), which combines VCI and TCI, detects rapid stress but often misses crop-specific water needs, response varies by vegetation type, and is less effective in irrigated areas where watering masks drought signals, and TCI generally contributes more than VCI in most regions (Zeng et al., 2022). Moreover, RS indices can be confounded by factors such as crop rotation and vegetation loss, necessitating robust field validation for accurate drought assessment.

Some indices, like the Temperature Vegetation Dryness Index (TVDI) and the Scaled Drought Condition Index (SDCI), improve flash drought monitoring by integrating temperature, vegetation, and precipitation data, but their effectiveness varies regionally. For instance, TVDI underperforms in humid regions and often requires dry-edge calibration in arid zones (Du et al., 2017). Meanwhile, SDCI accounts for various climatic conditions, i.e., humid, arid, and semi-arid areas; but model-based indices such as Crop Water Stress Index (CWSI), ESI, and TVDI generally respond better to sudden moisture deficits (Ma et al., 2021; Javed et al., 2021). Among these, the Evaporative Stress Index (ESI) (Anderson et al., 2013, 2016) and Standardized Evaporative Stress Ratio (SESR) (Christian et al., 2019) are widely used for agricultural drought assessment due to their ability to track rapid moisture fluctuations effectively. Complementary remote sensing indicators such as soil moisture, vegetation biomass, chlorophyll index, canopy or soil temperature, and surface water storage derived from thermal, optical, and microwave sensors further support vegetation stress monitoring (Wei et al., 2021; Liu et al., 2023; Vicente Serrano et al., 2023).

Biophysical indicators offer enhanced capability for early-stage flash drought detection by capturing subtle physiological changes that precede visible stress. For example, the Fraction of Absorbed Photosynthetically Active Radiation (fAPAR) serves as a proxy for photosynthetic activity; its reductions are closely linked to water stress and have been effective in discriminating low-yield years in Mediterranean Europe (Cammalleri et al., 2022). Solar-Induced Fluorescence (SIF), reflecting photosynthetic efficiency, can predict flash drought onset 2–8 weeks in advance via its rapid change index (RCI) (Mohammadi et al., 2022). Leaf Area Index (LAI) monitors structural biomass changes, although its sensitivity to seasonal dynamics and retrieval challenges limits routine uses in flash drought

monitoring (Hassanpour et al., 2024). Canopy Water Content (CWC), estimated from water-sensitive spectral bands (e.g., 970 nm, 1200 nm, 1450 nm, 1600 nm, 1940 nm, and 2500 nm), captures changes in plant water status and is useful when visible stress signs, such as browning or defoliation, are absent (Chai et al., 2020). It reflects the combined impact of atmospheric dryness, soil moisture, and plant drought tolerance (Zhang and Zhou, 2019). Alongside LAI and fAPAR, CWC captures cropland dynamics sensitive to agricultural practices, with strong alignment to field-scale observations (Hassanpour et al., 2024). However, CWC's application in flash drought contexts remains underexplored, requiring further testing and validation across case studies (Zhou et al., 2021). Among these indicators, only SIF is directly measured by satellites, while others are typically derived from optical data using statistical modeling, physical inversion techniques, or hybrid approaches that need ground validation and verification from other potential sources (Verrelst et al., 2015) which is important for their operational use for different regions and drought conditions.

Our study evaluated the predictive capacity of biophysical indicators (LAI, fAPAR, and CWC) derived from Sentinel-2 data to determine which indicator provides earlier drought signals compared to traditional indices such as the Evaporative Stress Index (ESI) and Normalized Difference Vegetation Index (NDVI). To capture the complex dynamics of flash droughts, we selected drought episodes varying in intensity, timing, and location, identified through ESI time series, to anchor our analysis on well-defined cases. We focused on testing the generalizability of the SL-2P algorithm for estimating biophysical traits across three cereal-dominated European regions: Southern Spain, Northern Italy, and Eastern Hungary. We selected wheat and maize-growing areas as major to strengthen the robustness of our approach for these key cereal crops. With that, we examined crop responses to drought stress across different phenological stages and assessed how early these responses can be detected remotely. Special attention was given to the spring 2023 and summer 2022 flash drought events, which coincided with critical developmental phases for spring wheat and summer maize. By mapping flash droughts through these biophysical indicators, we aim to enhance remote sensing-based decision support systems that facilitate real-time, targeted agricultural management. Our findings contribute to the development of proactive drought monitoring frameworks to mitigate flash drought impacts and protect crop yields.

2. Data and approach

Two flash drought episodes that differ in intensity, timing, duration, and geographic distribution are selected on the basis of ESI time series from 2018 to 2023 over three locations in Europe, shown with blue boxes in Fig. 1.

2.1. Study regions and drought cases

The total area of each ROI covered 25000 pixels, with each pixel measuring 20 m by 20 m, which gives a total of 10,000 km^2 per study site. The selection criteria are based on their frequent exposure to flash drought and agricultural context (Fig. 1).

ROI 1 lies in the Andalusia region of Southern Spain, which has a Mediterranean climate with hot, dry summers. The region experienced three consecutive years (2021–2023) of drought, with below-average rainfall (35 %) and extreme temperatures (up to 40 °C). Agriculture in Andalusia is heavily reliant on irrigation, where wheat, barley, and rice are largely grown. The groundwater

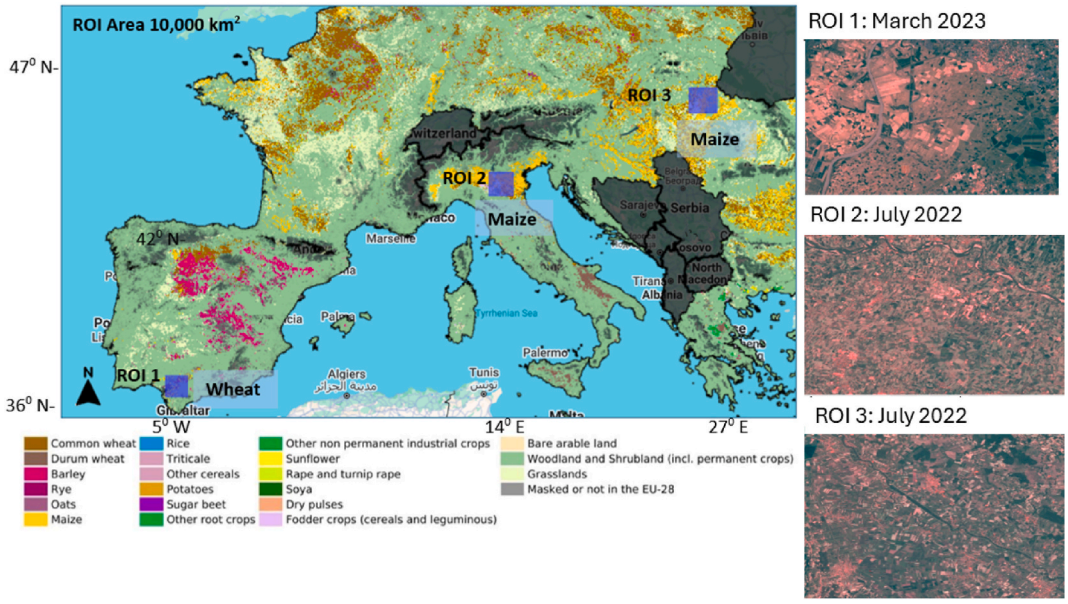

Fig. 1. The locations of three ROIs: Southern Spain (ROI 1), Northern Italy (ROI 2), and Eastern Hungary (ROI 3) overlaid on the ESA World Crop Map 2018 (d'Andrimont et al., 2021) with land use and land cover classes (wheat in brown and maize in yellow). To the right, zoomed RGB views from Sentinel-2 display agricultural fields within each ROI during the drought episodes of Spring 2023 and Summer 2022.

shortage in the Guadalete-Barbate River basin was a significant issue during this period, affecting their yields and putting pressure on the availability of water for irrigation (Martínez-Dalmau et al., 2023). Drought conditions have placed considerable strain on both the agriculture and the Guadalete-Barbate River flow.

ROI 2 is in the Po River Valley in Italy, which has a continental climate. It is one of Italy's most important agricultural areas in terms of maize production, mostly irrigated. They were heavily affected in 2022 by one of the worst droughts in over two centuries, when the Po River reached a historic low in the Summer of 2022. The event was worsened by altered precipitation patterns and increased agricultural water demands. The region's increased dependence on irrigation makes it particularly vulnerable to low water levels in the river (Monteleone and Borzí, 2024).

ROI 3 is in the Hungarian part of the Pannonian Basin, having a temperate climate with significant variability in summer rainfall. This region depends on rain-fed maize and barley and has experienced significant crop failures in past droughts due to variable and unpredictable rainfall, particularly during the summer months. Summer rainfall has considerable inter-annual variability, in July ranging from nearly 0 to 150 mm, and crop production is often susceptible to water shortages. Several severe droughts have been observed in the last two decades, i.e., 2003, 2007, 2012, 2015, 2017, and 2018, mostly exacerbated by low summer rainfall. This region is expected to continue facing significant droughts due to increasing climate unpredictability (Mohammadi et al., 2022; Mohammed et al., 2020).

2.2. *Evaporative Stress Index (ESI)*

For drought identification, we used the ready-to-use ESI product (available at https://gis1.servirglobal.net/data/esi/) that provides standardized global ESI change anomalies at 4- and 12-week scales. It expresses a weekly varying standardized anomaly (-2σ to 2σ) in fRET relative to long-term baseline conditions, highlighting areas with higher or lower-than-normal fRET during a week. Anomalies in actual ET and fRET, which is the ratio of actual ET (ETa) to reference ET (ETref) under clear-sky conditions, detect unusual changes in the ET process. fRET is calculated as follows.

$$fRET = \frac{ETa}{ETref} \tag{2}$$

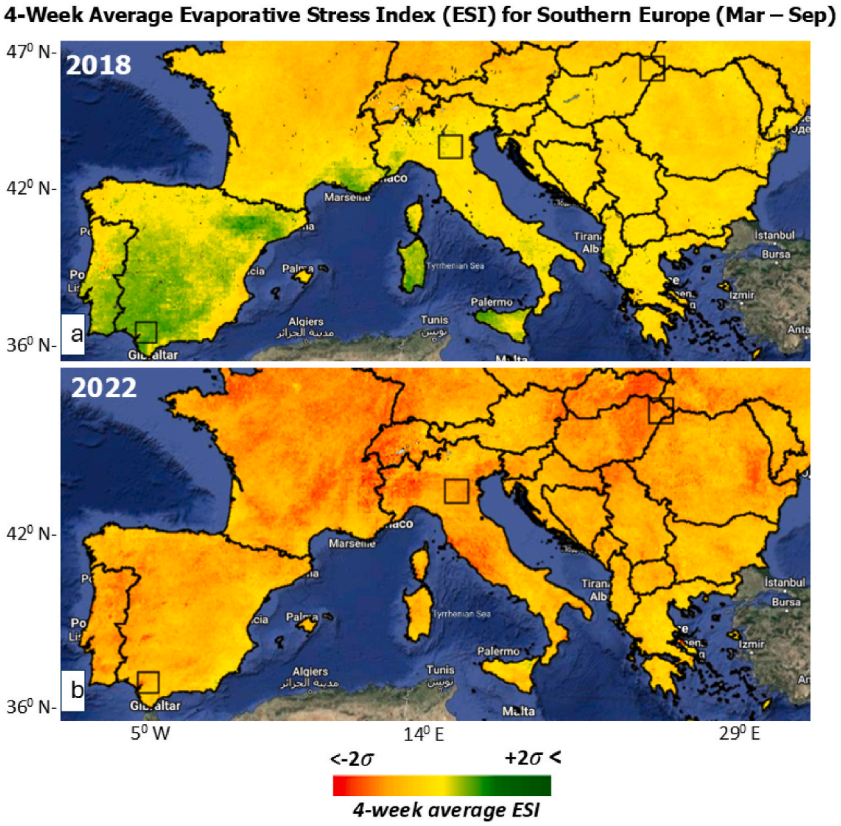

Fig. 2. The averaged ESI map from March to September for the years 2018 [] and 2022[b], highlighting the drought severity across the ROIs in 2022 compared to 2018.

Table 1
Displays the crop type for each ROI, crop-specific growing season, and selected years for comparative analysis.

ROIs	Crop	Growing Season	Drought Year	Non-Drought Year
ROI 1	Winter Wheat	1 Nov – 31 Aug	2023	2018
ROI 2	Spring Maize	1 Apr – 30 Nov	2022	2018
ROI 3	Spring Maize	1 Apr –30 Nov	2022	2023

Where: ETa is retrieved using ALEXI. ETref is Penman-Monteith FAO +56 (PM56) reference ET for grass (Allen et al., 1998). Normalization by ETref minimizes the influence of factors unrelated to soil moisture limitations, i.e., solar radiation and atmospheric demand.

ESI was chosen for its ability to capture agricultural drought at a 4 km resolution. It's a weekly product, based on temporal anomalies in fRET, and captures areas with anomalously high or low water use across the land surface. Unlike other drought indices, i.e., the Vegetation Health Index (VHI) or the Soil Moisture Anomaly Index (SAI), ESI effectively detects drought-affected areas by tracking ET variations driven by soil moisture limitations and can capture early signs of flash droughts from prolonged hot, dry, and windy conditions (Anderson et al., 2016; Shahzaman et al., 2021).

2.3. Selection of drought and non-drought cases

Fig. 2 displays the March to September averaged ESI for 2018 and 2022, captured areas where drought was severe. Notably, ESI in 2018 was above zero in scale over ROI 1 and ROI 2, indicating a normal year compared to ROI 3 (Fig. 2a), while year, 2022 was drier for all ROIs; intense drought conditions can be seen over ROI 2 and ROI 3 (Fig. 2b).

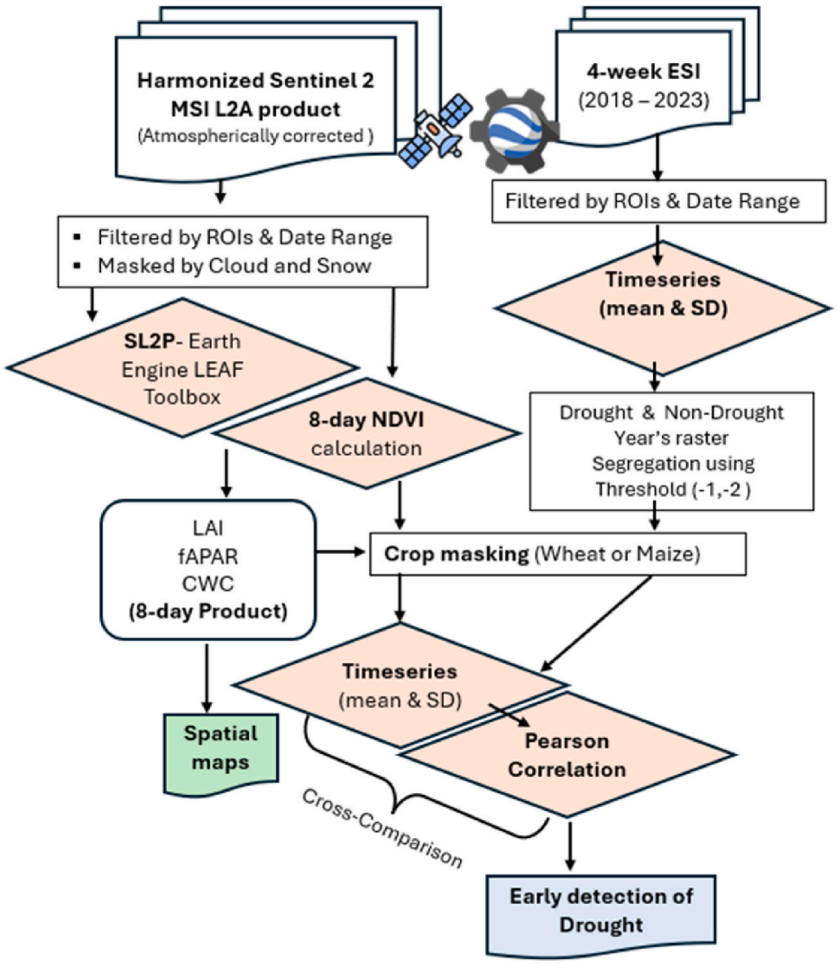

Fig. 3. Schematic view of analysis performed for comparison of SL2P-derived variables with ESI.

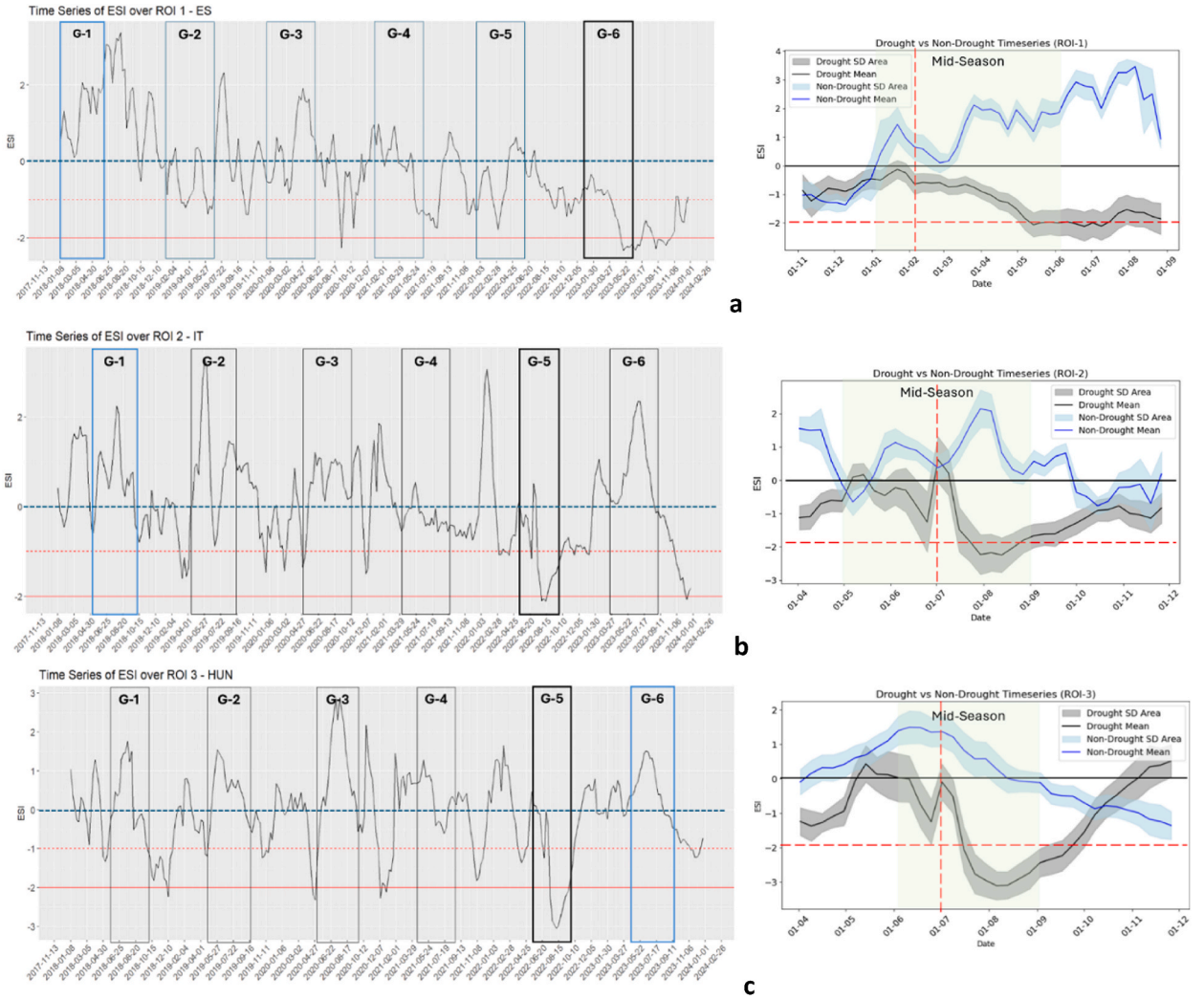

Fig. 4. Displays the ESI time series for six years (2018–2023) over ROI 1 in Southern Spain, **(a)** ROI 2 in Northern Italy, **(b)** ROI 3 in Eastern Hungary **(c)**, with the extreme drought episode highlighted with the black box and non-drought year as blue. G refers to the mid-season of the crops. Drought onset is identified when the ESI line crosses the -1σ threshold. The blue outline represents the non-drought year.

Further drought intensity was assessed from the ESI time series to check drought duration for the ROIs from 2018 to 2023, following the growing season window of the wheat and maize crop calendar for spring season. The drought and non-drought periods were defined for each ROI using a threshold technique. ESI thresholds of -2σ and -1σ were applied on time series to distinguish between mild water stress and severe drought across the study areas as strong negative values exceeding −1σ indicates dry conditions (Nguyen et al., 2019). Thresholding based on time series revealed spring 2023 as drought case for ROI 1 and summer 2022 as drought case for ROI 2 and 3. Similarly, threshold line above 1σ defined 2018 as non-drought year for ROI 1 and ROI 2 and year 2023 for ROI 3 when

Table 2
Describes the crop type of each ROI, selected years for comparison, onsets of droughts, and average ESI for the mid-season period of the crop during drought and normal years.

ROIs	Crop Type	Drought & Non-Drought Year	Mid-Season	Onset (ESI = −0.5)	Duration (Days)	Avg. ESI in Mid-Season of drought year	Avg. ESI in Mid-Season of non-Drought year
ROI 1: Southern Spain	Winter Wheat	(2023, 2018)	Jan–May	Feb 2, 2023	>30	−1.1	1.2
ROI 2: Northern Italy	Spring Maize	(2022,2018)	May–Aug	July 9, 2022	>30	−0.9	0.75
ROI 3: Eastern Hungary	Spring Maize	(2022,2023)	Jun–Aug	July 9, 2022	>30	−1.7	0.8

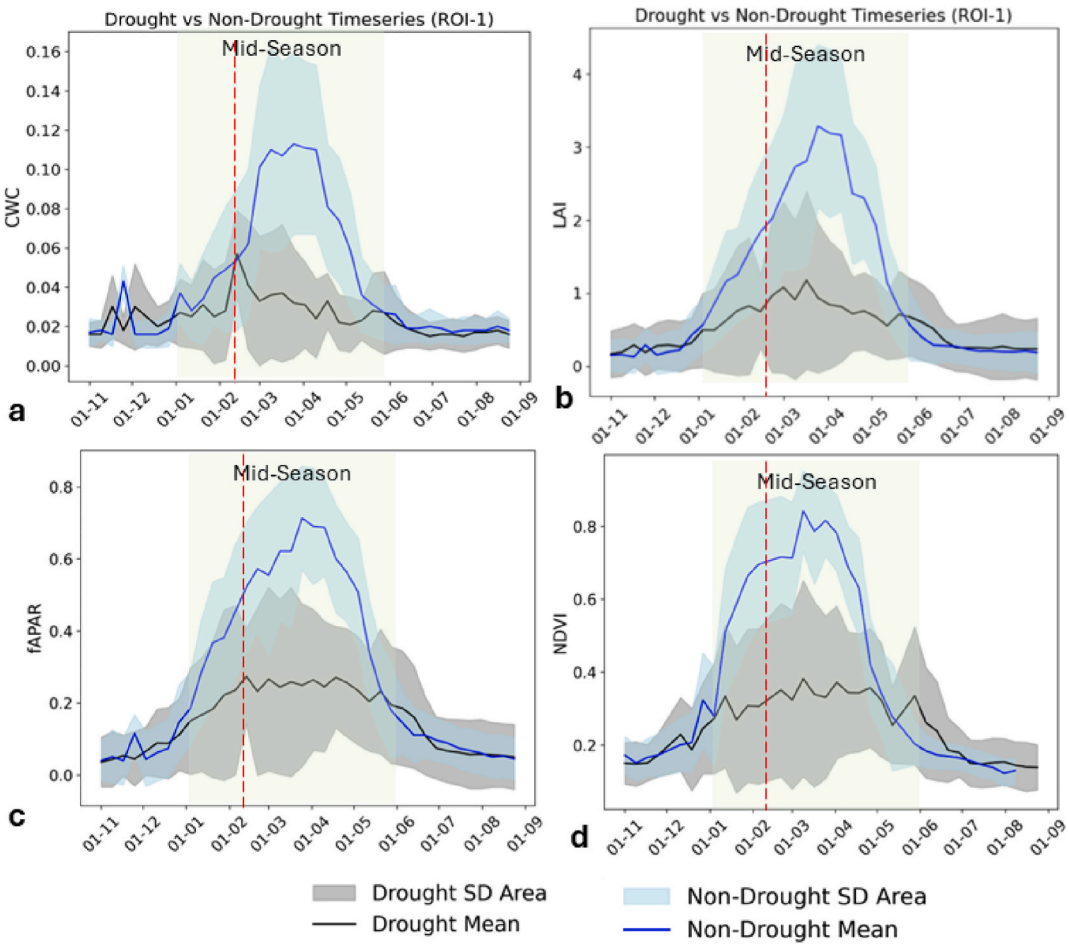

Fig. 5. 8-Day averaged Timeseries of CWC [a], LAI [b], fAPAR [c], and NDVI [d] along with standard deviation for the wheat growing season in both drought (in grey) and non-drought (in blue) years. The red line marks the onset of the flash drought detected in the ESI time series (February 2, 2023), and the green shaded area is the middle phase of wheat development, specifically the vegetative and reproductive stage (January–May).

ESI was above 1σ during summer, Table 1.

The initial screening of the ESI helped in identifying the onset, development, and persistence of flash droughts, which were then compared with the time series of biophysical variables and NDVI. Before delineating the time series for the selected drought cases, it was spatially verified that 100 % of the pixels within the ROI fell below the -2σ ESI threshold by the end of the crop growing season. The temporal window for the growing season was taken from the GIMMS-Global Agricultural Monitoring archive; details are in Appendix 1.

The time series of the ESI and biophysical variables were cross-compared to assess the ability of biophysical variables in providing an early indication of drought while capturing crop dynamics throughout the growth cycle from planting to harvest for both drought and non-drought years.

2.4. Generating data on crop biophysical variables

The primary dataset for generating biophysical variables was COPERNICUS/S2_SR_HARMONIZED, which provides atmospherically corrected harmonized surface reflectance data for Sentinel-2 imagery. For NDVI calculation, the Sentinel 2 archive was filtered to select images within the defined ROIs and temporal range. Images with more than 20 % cloud cover were excluded, ensuring that the analysis used only high-quality data. Further, the SCL (Scene Classification Layer) band from Sentinel-2 was used to identify and mask out cloud pixels. The median composite of all cloud-free S-2 images was computed for the selected period. The 8-day composite provided a more stable representation of crops' biophysical variables while reducing the data gaps caused by satellite revisit times and cloud contamination.

To derive canopy biophysical variables fAPAR, LAI, and CWC from Sentinel 2, we used a Sentinel 2 Level 2 Product Prototype Processor (SL2P)- LEAF toolbox v. 1 embedded in the Google Earth Engine (GEE). The data were processed according to the period

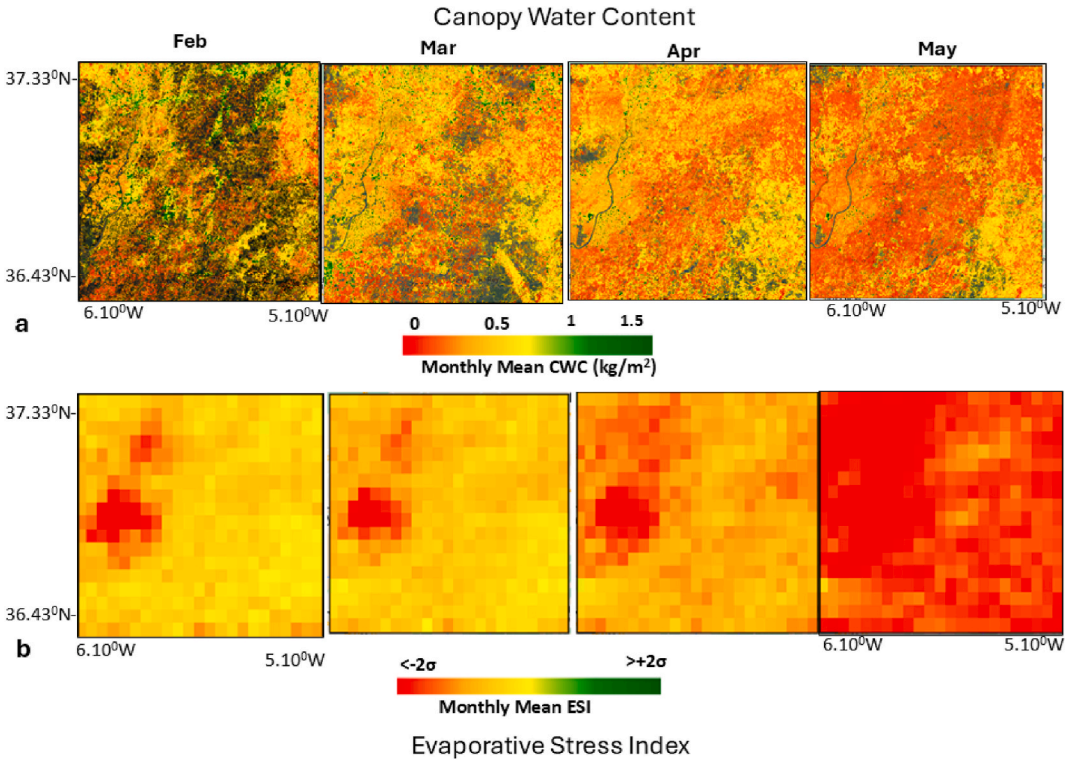

Fig. 6. Monthly CWC [a], and ESI [b] maps depicting the gradual increase of drought intensity by time. The grey areas on the CWC map indicate missing data from Sentinel-2 images due to cloud cover.

specified in Table 1. To ensure high-quality data, cloud-contaminated pixels were excluded using the LEAF Toolbox function called S2MaskClear. We then generated 8-day composites at a 20 m spatial resolution for each ROI, which represent the median of valid pixels and second mask, reprojectMaskAndExclude, was applied to remove low-quality pixels, with values below 0 excluded based on quality control (QC) flags to ensure reliable estimates of fAPAR, LAI, and CWC. The final product was further masked to isolate wheat and maize crop pixels, using the cereal mask from the ESA World Crop Map 2018 (d'Andrimont et al., 2021), and time series were delineated for analysis.

The theoretical foundation of the LEAF Toolbox Sentinel-2 Level 2 Processor (SL2P) is based on a backpropagation artificial neural network (ANN) trained on a globally representative dataset, which is simulated over the PROSAILH model. The PROSAILH model combines the SAIL (canopy bidirectional reflectance model) and PROSPECT (leaf reflectance and transmittance model) to simulate canopy reflectance across the spectral domain (Jacquemoud and Baret, 1990; Verhoef, 1984). It accounts for leaf optical properties, canopy structure, background reflectance, and illumination geometry (e.g., solar/view zenith and azimuth angles). The "H" in PROSAILH denotes its hybrid nature, allowing for more flexibility in simulating heterogeneous vegetation or complex canopy structures. SL2P uses two neural networks: The first predicts biophysical variables from input reflectance and acquisition geometry, while the second refines the predictions by modeling residuals. If the predicted values fall outside the valid range, they are either adjusted or flagged as invalid. The network is trained using both observed Sentinel-2 reflectance data and simulated reflectance spectra from PROSAILH, considering factors such as soil background, atmospheric conditions, and seasonal changes. Further details on the theoretical background and algorithm validation are in Fernandes et al. (2023) and Djamai et al. (2019).

2.5. Early detection potential assessed via time series & Pearson correlation

After masking non-wheat and non-maize pixels from 8-day composites, time series were generated and compared using the schema shown in Fig. 3. Temporal patterns were further filtered for crop pixels under extreme drought conditions, where the ESI was consistently below -2σ, to reconfirm the delineated patterns between biophysical variables (i.e., CWC, LAI, and fAPAR) and ESI across different levels of drought severity. This approach helps verify the potential ability of SL2P-based biophysical estimates to respond to flash droughts. The results for the -2σ threshold are in Appendix 2.

A simple Pearson correlation was calculated between the ESI and the time series of biophysical variables to measure the strength and direction of the linear relationship between them during both drought and non-drought years, following the equation.

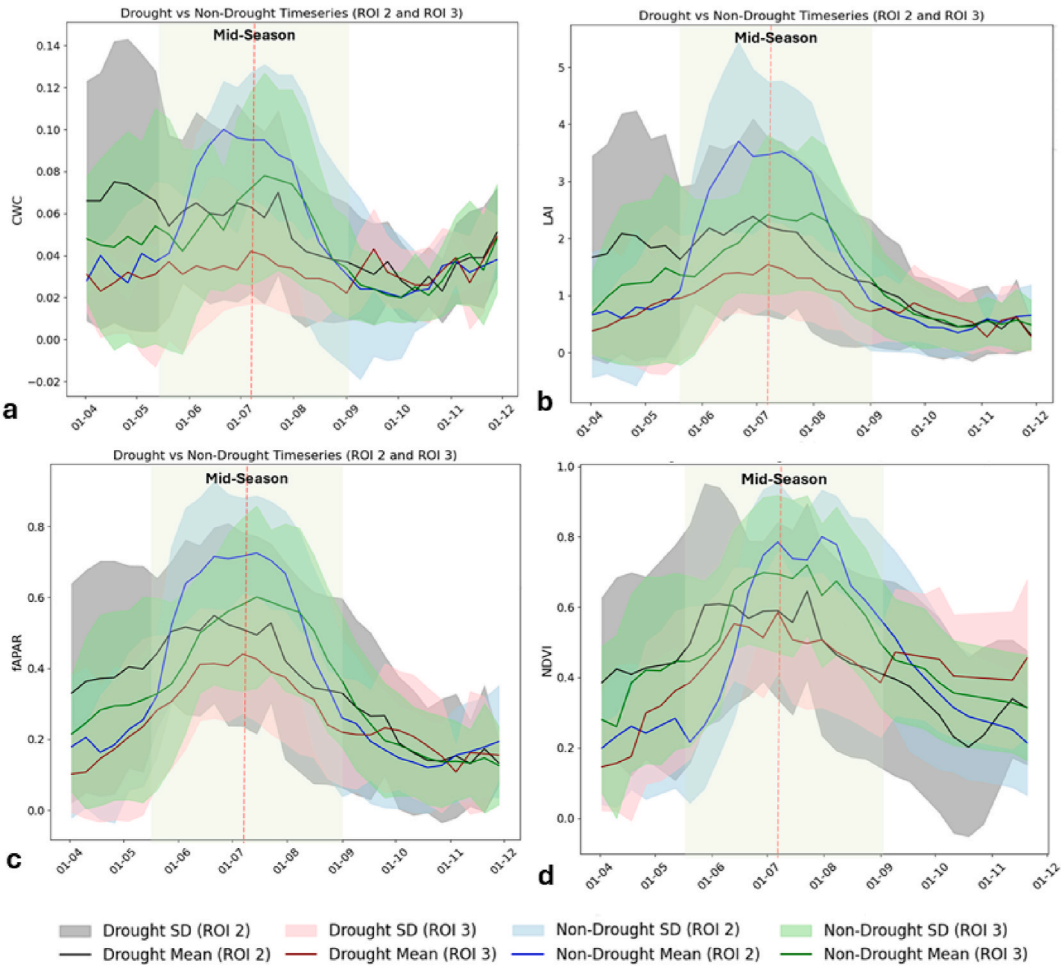

Fig. 7. 8-day averaged timeseries of CWC [a], LAI [b], fAPAR [c], and NDVI [d] along with standard deviation for the maize growing season in both drought and non-drought years of ROI 2 and ROI 3. The red line marks the onset of the flash drought detected in the ESI time series (July 9, 2022), and the green shaded area is the middle phase of maize development, covering the vegetative to grain-filling stage (May–August).

$$r = \frac{\sum_{i=1}^{n}(x_i - \overline{x})(y_i - \overline{y})}{\sqrt{\sum_{i=1}^{n}(x_i - \overline{x})^2}\sqrt{\sum_{i=1}^{n}(y_i - \overline{y})^2}} \tag{3}$$

Where:

n is the number of data points, x_i *and* y_i are the individual data points, $\overline{x}$ *and* $\overline{y}$ are the means of x and y.

3. Results

3.1. ESI time series from 2018 to 2023: identifying and characterizing flash drought events across ROIs

ESI time series at a 4-week scale encompassing six growing seasons of wheat designated as rectangles in ROI 1, and Maize in ROI 2 and 3. They were used to identify drought and non-drought years over the three ROIs from 2018 to 2023. Thresholds of -1σ and -2σ are used to determine the onset, duration, and intensity of drought events. The long-term ESI time series effectively distinguished between single and evolving events. In ROI 2, the ESI threshold of -1.5σ dropped in a single year, 2022, in Italy, while in other ROIs, the ESI threshold dropped below -1.5σ for consecutive years and became progressively more severe (Fig. 4). The temporal pattern and severity of these droughts were a bit different in all ROIs, depicting their climatic and geographical influences for each episode.

ROI 1- Southern Spain: The ESI time series in Fig. 4a from November 2017 to December 2023 showed a clear downward trend from 2018 onwards, culminating in the most severe and prolonged drought in Spring 2023. During this period, ESI dropped to -2σ and remained below this threshold for over six months (Feb–Aug 2023), coinciding with the wheat growing season. ESI began to decline in

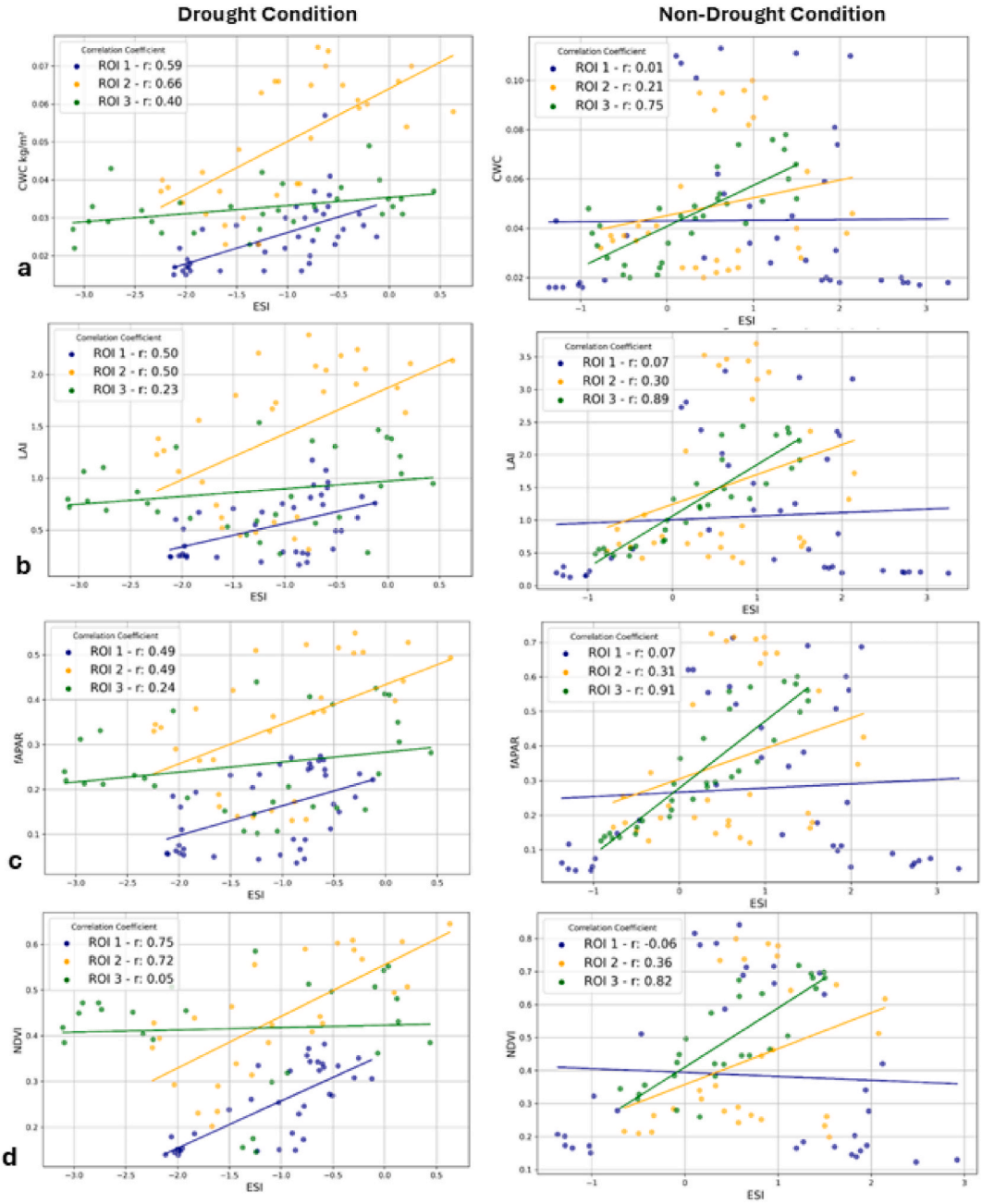

Fig. 8. Correlation between the mean values of CWC [a], LAI [b], fAPAR [c], and NDVI [d] with ESI in the crop growing season for both drought and non-drought years of all ROIs.

early February 2023 (in black), when wheat was in the emergence stage, and reached critical drought levels in May 2023, which corresponded with the peak growing period for wheat. On the other side, 2018 was a wet year throughout the growing season. ESI was within the 0 – 2σ range, indicating sufficient water availability to crops in the spring and summer months.

In 2019, ESI fluctuated between 0 and -1σ, depicting mild stress during the spring months, while summer 2021 observed moderate water stress with ESI near -1σ during summer. Despite a relatively less severe summer in 2022, notable water stress was observed in the winter of 2022, continuing into the next year (Fig. 4a). The ESI anomaly showed a gradual increase of drought risk in Andalusia due to the combined effect of rising temperatures, reduced rainfall, and higher ET, consistent with broader Mediterranean climatic trends (Hansel et al., 2022). The increasing frequency of droughts, as highlighted by the ESI trends, explained the vulnerability of the Andalusia region to extreme droughts.

ROI 2-Northern Italy: The severe drought of summer 2022 is obvious from the ESI time-series in Fig. 4b; it was the most intense

Table 3
Correlation between ESI and vegetation indicators during drought and non-drought year.

Drought					Non-drought				
ROIs	CWC	LAI	fAPAR	NDVI	ROIs	CWC	LAI	fAPAR	NDVI
ROI1	**0.59**	0.50	0.49	0.75	ROI1	0.01	0.07	0.07	−0.06
ROI2	**0.66**	0.50	0.49	0.72	ROI2	0.21	0.30	0.31	0.36
ROI3	**0.40**	0.23	0.24	0.05	ROI3	**0.75**	**0.89**	**0.91**	**0.82**

flash event in the last four years, gradually reaching the -2σ threshold in August, coinciding with the maize grain filling stage. The 2022 drought can be a flash drought, as it developed rapidly and reached critical scale -2σ in a month. Other less intense short-term droughts were also observed in 2019, 2020, and 2022, while 2018 and 2023 were relatively hydrologically stable years, so 2018 was selected as a non-drought year for comparison with the drought year 2022.

ROI 3- Eastern Hungary (ROI 3): As obvious from the time series in Fig. 4c, the drought began in July 2022, coinciding with the maize crop's critical growth period, and persisted until October 2022. The ESI threshold was persistently lower than -3σ in the entire months of August and September, highlighting severity higher than in Italy and Spain. For the ROI 3 comparison, the year 2023 was selected as the year of non-drought, and 2022 was selected as the year of extreme drought.

For ROIs 2 and 3, drought occurred in the same month. The ESI rapidly declined from 0.5 to -2σ in ROI 2 and from 0.5 to -3σ in ROI 3, signaling the rapid onset in July and development in August. In ROI 3, the drought conditions started to recover in November, with ESI increasing over time. However, in ROI 2, ESI remained below -1σ throughout the timeframe, indicating that drought persisted longer than ROI 3.

Table 2 shows the onset of each drought for ROIs, onset defined by a threshold of -0.5σ. The crop-specific mid-season time window and drought onset date were used to compare biophysical variables response with ESI. The average ESI indicates that the drought in ROI 3 was the most intense, with an average ESI of -1.7σ. This is further evident from the ESI time series for ROI 3 (Fig. 4c), which shows ESI values below -3σ during the month of August, the most severe case. All chosen drought cases have a duration above 1 month at a -1σ severity scale.

3.2. Comparison of biophysical variable in detecting drought onset in RO I 1

Fig. 5 presents CWC, LAI, fAPAR, and NDVI time series covering the winter wheat phenology for 2023 (drought) and 2018 (non-drought) year, from 1st November to 31st August of the following year. This timeframe covers both the sowing and harvesting periods.

All biophysical variables and NDVI displayed a typical phenology curve in the non-drought year of 2018. Defining the phenology, in a normal year, the wheat crop begins to establish in February and enters the vegetative growth stage by March. The crop reaches its full development stage in May 2018 after senescence. This pattern is indicated by canopy biophysical variables and NDVI, showing normal crop growth and healthy photosynthetic activity under adequate moisture conditions in which LAI reaches 3, fAPAR up to 0.7, NDVI 0.8, and CWC 0.1 in March and April, when the crop is in its late vegetative and reproductive phase.

During the drought year (2023), significant change was observed in the phenology curve with a decline in the magnitude of LAI, fAPAR, and CWC, indicating that crops struggled to establish after the drought onset. Among the three biophysical variables and NDVI, CWC showed the earliest decline (Feb. 2, 2023) during the wheat establishment phase, and this decline continued throughout the crop season in parallel to ESI (Fig. 5a). Similarly, both LAI and fAPAR remained at lower levels, with fAPAR around 0.2 and LAI in the range of 1 during the mid-growing season (Fig. 5b and c). In a non-drought year, LAI peaked at around 3, NDVI peaked at 0.8 and fAPAR at 0.7, but in the drought year, they were reduced to 1, 0.3 and 0.2, indicating poor crop health. It showed that crop health was significantly affected, with noticeable changes in crop structure and photosynthetic efficiency. Their steady declining response signals deteriorating crop performance until the harvest stage in May.

However, there is a clear indication of CWC declining in February 2023, which reflected a soil moisture deficit at the sowing and emergence stage, when seeds needed sufficient water to germinate. The CWC decline aligned well with the ESI's indication of flash drought onset in February with one-week lagged response (Fig. 4a) during the early spring period of 2023. The sharp decline in CWC at first and throughout the growing season indicated the strong response signal. Compared to CWC, NDVI, LAI and fAPAR were steady and less indicative of capturing the onset of drought (Fig. 5 b, c, d).

We further verified this pattern by screening pixels where ESI reached -2σ and -3σ to test only for drought-prone areas. Biophysical time series for each variable were then delineated for both drought and non-drought years, following a similar approach (Fig. 3). This supplementary analysis confirmed the similar phenology pattern: the maximum average LAI during the drought year did not exceed 1, indicating that crops in these areas failed to develop. The fAPAR was also lower due to the drought. CWC exhibited a similar trend, declining from February 2023, indicating insufficient water availability for crops. These graphs for the -2σ thresholds are provided in the Fig. 9, Appendix 2.

Besides timeseries, monthly averaged maps of CWC and ESI during drought also showed spatial dynamics of CWC aligned with ESI (Fig. 6b). Declining CWC values from 1.5 to 0 kg/m^2, as shown in Fig. 6a, reflected the physiological stress experienced by crops during drought onset and stalled development. These maps demonstrated how CWC and ESI reflected the same drought occurrence pattern in Andalusia in 2023. Fields that initially had values in the range of 1–1.5 kg/m^2, indicating adequate water, transitioned to red as CWC diminished, reflecting visible signs of canopy water loss. This transition signalled the strong impact of drought, from its onset to gradually increasing severity. When using the ESI for crops at a 4 km resolution, it's difficult to interpret stress at the field level. In

contrast, the SL2P-derived CWC at 20 m resolution can show a field scale view, which is useful for assessing fields individually. This approach can be useful for diverse and fragmented landscapes.

3.3. Comparison of biophysical variable in detecting drought onset in ROI 2 and 3

Fig. 7 presents CWC, LAI, fAPAR, and NDVI time series covering the maize phenology for 2022 (drought) and 2018 (non-drought) year for ROI 2 and 2023 (non-drought) year for ROI 3, from 1st April to 30th November. This timeframe covers both the sowing and harvesting periods of Maize.

In ROI 2 and 3, the sowing of spring maize typically takes place in March, with seed germination occurring in warmer temperatures. From April to June, adequate moisture is required to support its key vegetative stages, including leaf development, stem elongation, and root expansion. This is critical as maize is highly sensitive to water stress during these stages. The vegetative phase culminates in the tasselling stage, from which reproductive development begins. During the flowering, pollination, and grain-filling stages from May to July, the water demand of maize is especially high, as these stages are crucial for yield formation. Water is essential for successful pollination and kernel development. Maize reaches full maturity by late July to early August; at this stage, water requirements decrease as the crop transitions into physiological maturity, with kernels hardening and the crop drying in preparation for harvest in September onwards. Therefore, water availability is crucial from April to July as drought stress during this period can negatively affect final yield and kernel quality.

The phenological development of maize in ROI 2 (North Italy) in 2018 and ROI 3 (Southern Hungary) in 2023 was captured through time series data of CWC, LAI, fAPAR, and NDVI. These time series in Fig. 7 reveal the variations in growth patterns between the regions. For ROI 2, the peak of vegetative health indicators, such as CWC, LAI, fAPAR, and NDVI, can be seen around June, compared to ROI 3, where the peak of the indicators is in July. This one-month difference reflects the different seasonal lengths and growth patterns of the maize between the two regions. The rainfed maize is sown in April and reaches peak maturity by August. So, July is a critical month for both irrigated and rainfed maize.

In Fig. 7a and d, NDVI and CWC of rainfed maize in ROI 3 are lower than irrigated maize in ROI 2, primarily due to drier conditions in ROI 3, which leads to reduced chlorophyll content, a lower LAI, a reduced fAPAR, and, consequently, lower photosynthetic potential. While water availability plays a significant role in these differences, other factors, such as soil type, temperature, and nutrient availability, also contribute to the variation in vegetation health indicators between rainfed and irrigated maize. Overall, ROI 3 (Southern Hungary) has a shorter seasonal length for maize compared to ROI 2 (North Italy), and it experiences water-limited conditions in summer, leading to lower vegetation health and indicating its lower yield potential. The time series of non-drought years (2018 and 2023) showed irrigated maize has better leaf area and active photosynthesis in the June to August peak growing time, reflecting ample water availability.

Drought on-set in July 2022 during the reproductive and grain-filling stage significantly impacted the crop with high water demand, as seen in the biophysical variables and NDVI time series (Fig. 7). Both LAI and fAPAR steadily declined in June and July (Fig. 7b and c). It is already known that the mid-season drought occurring during key development stages can affect crop health, especially drought during flowering and grain-filling stages, which can severely reduce yield (Vicente-Serrano et al., 2013)

A sharp drop in CWC was recorded in early July in ROI 3, coinciding with drought onset, which caused the average LAI to fall below 2. The significant drop in CWC and fAPAR, alongside the declining trends in LAI and NDVI in both ROIs, showed that the drought affected the crop during its maturity phase. As drought conditions worsened in August (Fig. 4b,c), biophysical variables showed significant declines and erratic responses, indicating that maize development was adversely affected by the drought. The diminishing canopy structure in ROI 2 reflected by LAI declined from 2, photosynthetic activity also reduced from 0.6 to 0.4 and NDVI below 0.6. The change in their average magnitude confirmed that crops could not grow well in July. As drought onset was in the middle of the grain-filling stage, maize was short of adequate water for its proper growth.

Our results showed that the CWC decline was consistent with ESI, from the first week of July and continuing to decline throughout August, indicating its high sensitivity to drought stress (Fig. 7a). For example, ESI in ROI 3 began to decline on 9 July from -0.5 to -2σ on 16 July (Fig. 4c). CWC reduced from 0.04 on 14 Jul to 0.02 until August, LAI also declined from 1.4 to 0.7 and fAPAR from 0.4 to 0.2 from mid-July to August. These declines reflect maize's inability to maintain healthy growth under extreme drought conditions, particularly during its critical maturity phase in July and August.

Spatial averages of CWC, LAI, fAPAR, and NDVI all showed significant reductions under drought conditions, further highlighting the negative impact of drought on productivity. Our findings align with those of Lawal et al. (2022), who observed LAI decline in response to drought characterized by SPEI in central and southeastern Southern Africa. Our results revealed that drought response for Italy and Hungary was consistent for key biophysical variables, with changes occurring promptly after drought onset. The response of these variables was further validated by analysing crop pixels steadily exposed to extreme (ESI values of -2σ and -3σ), which reduced the pixel sample size. However, the mean trends still showed a similar change in phenological response across all variables for maize, as observed in Fig. 7.

3.4. Correlation between ESI and crop variables

The relationship between crop variables and the ESI was verified using Pearson correlation analysis among time series of both drought and non-drought periods. During the drought year, the variables NDVI and CWC in ROI 1 and ROI 2 exhibited a strong positive correlation with ESI, reflecting their sensitivity to drought stress. Specifically, NDVI showed correlations of $r = 0.75$ in ROI 1 and $r = 0.72$ in ROI 2, while CWC showed correlations of $r = 0.59$ in ROI 1 and $r = 0.66$ in ROI 2 (Fig. 8, Table 3) (see Fig. 9).

These higher correlation values suggest that NDVI and CWC are more responsive to changes in ESI, which is indicative of drought stress. The persistent drought conditions likely made crop variables like NDVI and CWC highly sensitive to ESI. The strong correlation between CWC and ESI during the drought period is expected, as drought typically leads to reduced soil moisture and transpiration rates, creating water stress that impacts plant physiology (Lyons et al., 2021). As both ROI 1 and ROI 2 rely heavily on irrigation, water availability is directly tied to crop health, making crops in these regions more responsive to ESI.

In contrast, LAI and fAPAR had slightly weaker correlations, with $r = 0.50$ for LAI and $r = 0.49$ for fAPAR in both ROIs (Fig. 8b and c). This suggests that while these variables are still related to ESI, they are less sensitive to drought stress compared to NDVI and CWC. The relatively lower correlation for LAI and fAPAR could be because these variables can be influenced by other factors beyond drought stress, such as nutrient availability, which may weaken their direct relationship with ESI.

In ROI 3, the relationships between vegetation indicators and ESI were notably weaker for the drought case. NDVI showed a very low correlation ($r = 0.05$), indicating that NDVI was almost unaffected by drought conditions in this region. This could be because ROI 3, which is rainfed, may have different growth dynamics compared to the irrigated regions (ROI 1 and ROI 2). The other variables in ROI 3 also showed relatively low correlations with ESI: LAI ($r = 0.23$) and fAPAR ($r = 0.24$) except CWC ($r = 0.40$); still, it showed a noticeable relation with ESI (Table 3). However, weak correlations suggest that the impact of drought on maize in ROI 3 may not have been as pronounced or uniform as in ROI 1 and ROI 2, possibly due to the regional differences in drought tolerance. Overall, these results indicate that CWC is more sensitive and closely linked to ESI, particularly in the irrigated regions.

Crop health responses to drought stress can differ depending on climatic conditions, agricultural practices, and water management strategies in each region. ROI3 region has perhaps developed adaptive mechanisms to cope with varying water availability. As a result, the crop variables may not be as closely linked to ESI because the crops are not under consistent irrigation stress, and the rainfed system introduces additional variability in crop performance based on the timing and amount of rainfall. This could explain why the correlation between ESI and vegetation indicators was weaker in ROI 3 compared to ROI 1 and ROI 2.

During the non-drought year, the correlations between vegetation indicators (NDVI, CWC, LAI, and fAPAR) and the positive ESI were noticeably different than during the drought year. The strong positive correlations with ESI during the non-drought year (NDVI: $r = 0.82$, CWC: $r = 0.75$, LAI: $r = 0.89$, fAPAR: $r = 0.91$) are likely because, in regions with rainfed agriculture, even slight changes in water availability can lead to noticeable changes in crop health. In 2023, sufficient rainfall might lead to optimal conditions for crop growth, making these variables strongly correlated with ESI and indicating good water conditions and healthy vegetation. Consequently, the ESI pattern closely coincides with the phenology detected by biophysical variables, such as crop development and leaf area, which are directly influenced by water availability. This synchronicity reflects how well-watered conditions facilitate the growth and health of crops, making these vegetation indicators strongly aligned with the ESI.

4. Discussion

In this study, we compared biophysical variables (CWC, LAI, and fAPAR) and NDVI with ESI to evaluate how early these variables respond to flash droughts, taking three case studies of Southern Spain, North Italy, and Eastern Hungary. Our findings revealed that compared to other biophysical variables, CWC showed the earliest as well as a pronounced decline at the onset of flash droughts. The early detection of drought is most prominent in the semi-arid irrigated region of ROI 1 in Spain for the Spring drought in 2023.

4.1. CWC as an early indicator of flash drought

The congruence between CWC and ESI during drought periods was expected, as drought typically leads to reduced soil moisture and transpiration rates, resulting in water stress that affects plant physiological processes (Lyons et al., 2021). CWC effectively captures this physiological impact of water stress due to its reliance on leaf water content, which decreases under water-limited conditions. This indicates that, unlike visible symptoms, CWC can detect non-visible impacts on vegetation functioning. Its responsiveness to these physiological changes makes it a valuable indicator for drought assessment. This ability to detect early signs of water stress is crucial, as failure to identify and manage instantaneous water stress promptly can lead to long-term damage to crops (Sungmin and Park, 2023), and we also observed in our case studies on mid-season drought, prolonged water stress can have lasting impacts on plant physiology, health, and productivity. As drought severely reduces water availability, it affects CWC more quickly, and crops struggle to maintain normal transpiration rates.

4.2. CWC response relative to NDVI, LAI, and fAPAR

Looking into crop water dynamics through CWC, which responds quickly to water stress, the response of LAI and fAPAR to drought was either delayed or more subtle. During drought conditions, the correlations between ESI and other variables (LAI and fAPAR) were also weaker. These variables do not immediately reflect changes in water availability; instead, their effects accumulate over time, which means longer timescales (monthly or seasonal) are required for meaningful drought-related changes to appear. Kim et al. (2017) found a strong relationship between LAI and SPEI over 9–12-month periods under the cumulative effects of drought. This slow buildup contrasts with the more immediate changes seen in CWC, proving that CWC is more sensitive to short-term water availability fluctuations. Usually, in the case of LAI, the response to water stress takes time to manifest. This delayed response in LAI and fAPAR contrasts with the more immediate changes in CWC, highlighting the differences in how these variables reflect the impact of drought. Both LAI and fAPAR do not fully capture the immediate impacts of drought and are indirect indicators of vegetation health. Whereas CWC is a direct biotic driver, with changes in CWC quickly affecting spectral vegetation indices like NDVI and NDWI (Zhou et al.,

2022). Our results also showed that as drought intensified, CWC exhibited a continued dropping signal, whereas the response from LAI and fAPAR was steady.

Other studies also noticed that in the farming ecosystems where soil moisture deficit is the primary stressor, biomass-related indices such as NDVI, PRI, LAI, and fAPAR tend to be less responsive than CWC (Vicca et al., 2016; Lawal et al., 2022; Cammalleri et al., 2022). These indicators are less effective at capturing the rapid changes in plant water status that occur during drought conditions. In contrast, CWC responds more sensitively to variations in soil moisture. Our research acknowledges that the rapid response of CWC to drought is due to soil moisture changes. Our findings are consistent with Zhang and Zhou (2019), which indicated that CWC is influenced by soil water status and crop developmental stage. Compared to LAI, CWC is a rapid and reliable indicator due to its prominent drop during critical growth stages of the crops. It can be effective for irrigation planning during the emergence and senescence stages and can be used as a proxy for crop health, which can help farmers and agronomists to optimize water management strategies to sustain yields, especially in irrigated areas.

4.3. Applicability of CWC across different crop types and climatic conditions

Consolidating the use of CWC for early detection requires further validation in agricultural settings to ensure its efficacy in drought monitoring. Since crop water status is closely linked to changes in photosynthesis and transpiration during drought conditions, it plays a crucial role in determining biomass production and yield. As plants begin to conserve water, they exhibit more pronounced signs of drought stress, including reduced leaf turgor and altered leaf water content, so the CWC response is prominent. However, validation of the CWC response in various crops will provide a piece of valuable information for drought impact assessment in agriculture.

Assessing the impact of drought on crops can be complex, as the response varies depending on the specific growth stage at which the drought occurs. Our study has proven that impact is detectable through CWC during critical growth stages, such as emergence and grain-filling, when sufficient water is essential for seed germination and grain richness. Other research, such as Barros et al. (2020), also showed that droughts during different growth stages affect crops differently. CWC can be a reliable drought indicator if more crop-specific observations are made, particularly to ensure its reliability for early detection. However, this assessment can be challenging in arid ecosystems, where crops also exhibit stress memory, allowing them to learn from past droughts and better withstand future stress. This memory involves changes in gene expression influenced by epigenetic and molecular mechanisms (Kambona et al., 2023). These physiological adaptations might be reflected in a weaker response of CWC to drought in a rain-fed environment. Moreover, CWC is more tightly coupled with soil moisture during drought conditions, and this relationship varies across different climates. Lyons et al. (2021) noticed that in humid regions with less climatic variability, CWC is not influenced by soil moisture. In areas with intermediate climatic water deficits, where atmospheric water demand and soil moisture are more tightly linked, CWC shows greater sensitivity (Lyons et al., 2021). Therefore, more targeted field studies are essential to understand CWC's limitations and potential across various crop types and climatic conditions to inform effective drought monitoring and management strategies that consider regional variations in climate, vegetation, and hydrology using holistic approaches.

4.4. Differences in CWC responses between irrigated and rainfed systems

In the non-drought year 2023, a strong correlation between ESI and biophysical variables was observed in the rainfed maize areas of Hungary (ROI 3). However, in ROI 1 and ROI 2, the patterns shifted during the drought year. This shows the variability in crop response to water stress across different regions, with rainfed crops (like those in ROI 3) potentially exhibiting greater adaptation to water-limited conditions. In these areas, even slight changes in water availability can result in noticeable changes in crop health, making CWC a potential indicator for detecting early signs of water stress.

ROI 1 and ROI 2, with their reliance on irrigation, experienced exacerbated stress during drought years due to irrigation limitations. The severe droughts of summer 2022 and spring 2023 revealed the vulnerability of irrigation-dependent agriculture, where reduced water availability had a significant impact on crop health. CWC performance (Figs. 5–7) indicates that as irrigation water availability becomes constrained, its monitoring can be effective for detecting agricultural risks. Considering that even if a crop appears unaffected by drought, its functioning can still be impaired, accurate real-time monitoring of CWC can enhance agricultural water use efficiency. Field studies on maize in the summer showed that CWC is a more sensitive and reliable indicator of crop water stress compared to other indicators like leaf equivalent water thickness (EWT) and live fuel moisture content (LFMC). Others have accounted for crop growth and development information alongside CWC to improve crop water prediction through hyperspectral indices (Pasqualotto et al., 2018; Zhang and Zhou, 2019).

Monitoring pre-drought soil moisture conditions is equally important for rainfed and irrigated regions, as rapid transitions to water-stressed conditions can lead to a sharp decline in vegetation health and the photosynthetic capacity of the crops if water stress occurs within weeks, then soil moisture can also explain the differing sensitivity of CWC to drought stress in rain-fed versus irrigated systems at a large scale (Sungmin and Park, 2023). At the onset of drought, as soil moisture declines, CWC decreases sharply, leading to reduced transpiration and stomatal conductance; however, the response varies by drought emergence at different crop stages (Qiao et al., 2024).

Our analysis was focused on developing a proactive drought detection approach that can give a timely assessment of drought impacts during critical times of crop growth. By proactively addressing drought conditions, we can avoid costly measures, such as installing new irrigation systems, expanding water supplies, or making heavy investments in replanting and soil health reclamation.

4.5. CWC application in proactive drought detection

Long-term soil moisture data can be useful for assessing general trends in water availability, but it lacks the sensitivity required to detect rapid, short-term changes in crop water stress. Soil Moisture Active Passive (SMAP) data provide critical information on soil moisture retention, especially at the root depth zone (30 cm), and their changes capture changes in drought intensity levels over 13- to 26-week intervals (Sehgal et al., 2021; Eswar et al., 2018). While SMAP captures soil moisture dynamics, CWC reflects the actual physiological state of the plant, offering a complementary, more direct tool for assessing crop stress and predicting drought impacts on yield. This makes CWC a valuable tool for the earlier detection of water stress and more precise drought monitoring, especially in situations where drought evolves rapidly or affects crop health more quickly than soil moisture dynamics.

Other drought indices such as Precipitation Condition Index (PCI), the Soil Moisture Condition Index (SMCI), the Vegetation Condition Index (VCI), and the Temperature Condition Index (TCI) track changes in precipitation, soil moisture, vegetation health, and temperature over time, they typically provide indirect indicators of drought and vegetation stress. These indices are often normalized on a scale of 0–1 for ease of comparison together (Jiao et al., 2016; Ahmadi et al., 2022). They can lack the sensitivity required to detect subtle, short-term changes in crop water status. Moreover, these indices typically capture broader environmental conditions and may not reflect immediate changes in plant physiology.

For early detection of drought stress on vegetation, RS Platforms, like the Global Integrated Drought Monitoring and Prediction System (GIDMaPS) by the University of California- Irvine (UCI), South Asia Drought Monitoring System (SADMS) by International Water Management Institute (IWMI), uses suite of vegetation indicators to monitor droughts (Bachmair et al., 2016). Such drought monitoring systems offer the advantage of real-time, high-resolution monitoring, allowing stakeholders to take proactive measures and improving decision-making and response times in agriculture, water management, and disaster mitigation. The European Drought Observatory developed a Combined Drought Indicator (CDI) based on fAPAR to detect drought at early stages before it escalates into severe conditions (Sepulcre-Canto et al., 2012). As flash drought conditions evolve quickly, the short period of drought episodes necessitates the need for higher temporal resolution (e.g., frequent satellite overpasses) and real-time crop stress detection. Infrequent observations will miss early signs of drought stress or lead to inaccurate assessments of crop conditions. Combining indicators that capture both structural and functional responses to drought, with high temporal resolution, can develop a better proactive drought detection system. In future, the operational delivery of early-in-end-of-season, high-resolution response indicator maps from the local scale to the global scale using integrated Earth Observation (EO) systems (e.g., ECOSTRESS, SMAP, Copernicus Sentinel 2, and upcoming missions such as HiVE, FORUM, CHIME, FLEX) would be an advantage for flash drought monitoring and management.

5. Limitations

Our study acknowledges that crop-specific CWC responses to drought require further investigation, given that different cereal crops exhibit varying degrees of drought resistance or susceptibility, which may affect the utility of CWC as a consistent indicator across crops (Dao et al., 2021; Genangeli et al., 2023). However, we addressed this limitation by focusing on two cereal crops (wheat and maize) in two cropping systems (irrigated and rainfed) to assess CWC's ability to reflect drought stress in both systems. Through this approach, we evaluated CWC's sensitivity and reliability as an indicator of drought in diverse agricultural contexts. We also compared CWC performance with other established drought indicators, like LAI and fAPAR, to better understand its strengths and weaknesses in different crop systems. However, the differences in how CWC reflects crop behaviour in irrigated and rainfed systems require more in-depth canopy-scale studies to better understand its behavior under different water availability conditions, such as erratic rainfall, sprinkler irrigation, water logging, etc.

The lack of extensive validation of CWC across different ecosystems contributes to uncertainty regarding its broader applicability. Previous research in the Canadian Prairies has shown that CWC performed less effectively compared to other variables, i.e., LAI and fCover, indicating potential biases in its accuracy, so confidence in SL2P-based CWC is low (Djamai et al., 2019). Also, there is no standard protocol for CWC that could translate its quantitative assessment into drought severity classification for different cropping systems. The lack of standardization can complicate CWC comparisons across regions, periods, and deriving methods. Whereas LAI and fAPAR have been validated for various ecosystems in different contexts (Fernandes et al., 2023). Our study is pioneering in that CWC has not yet been validated across diverse environmental contexts, which is now contributing to strengthening its reliability and potential use as a drought monitoring tool. Our study has realized that the CWC is not in the list of essential climate variables (ECVs), whereas LAI and fAPAR are among 55 ECVs (Baret et al., 2013). Future research on CWC can further consolidate its potential use in flash drought detection and can define severity scales for improved drought detection, such as FAO's Agriculture Stress Index system has done (FAO, 2016).

One key challenge in relying on SL2P-based CWC could be persistent cloud cover that can limit its effectiveness for flash drought monitoring. Another could be variability of environmental and canopy characteristics due to differing growth conditions. As crops can have different leaf structures, stomatal conductance, and canopy densities, leading to varying levels of CWC even under similar environmental conditions, which needs attention in the general applicability of SL2P-based CWC estimates across diverse agricultural areas. In addition to cloud cover, the SL2P data processing applies quality control masks that exclude pixels with invalid values, which can reduce spatial completeness and affect the time series. SL2P biophysical variable retrieval relies on neural networks trained on simulated canopy reflectance data, which may introduce uncertainties when applied to heterogeneous landscapes. The revisit frequency of Sentinel-2 satellites, combined with cloud contamination, can cause temporal gaps that challenge the detection of short-term flash drought events for some locations, although our study framework appeared robust for our locations in addressing these challenges.

As realized in this study, CWC may exhibit a lagged response to soil moisture deficits due to the time required for stress signals to propagate from the root zone to the canopy, and this lag can vary by canopy height and the crop's phenological profiles. A lag in CWC response, with deeper root systems or anisohydric behavior of the crops, can also limit the effectiveness of CWC, particularly in the early phases of drought onset. Moreover, crop management practices, such as irrigation scheduling or fertilization, may also influence biophysical variable responses independently of drought stress.

We used the ESI to determine the occurrence of flash droughts due to its high temporal resolution. The thresholds used to define drought severity (-1σ, -2σ), while based on prior literature, are somewhat arbitrary and may not perfectly delineate mild and severe drought conditions across the globe. Future work should explore adaptive or region-specific thresholds calibrated with crop phenology and yield data to improve flash drought classification. Moreover, ESI itself has some limitations. Cloud cover, particularly during the spring and early summer crop growing season, can introduce data gaps or reduce the accuracy of rapid ET changes, which can impact the index's ability to provide reliable flash drought signals. In our case studies, ESI performed well in the growing seasons of wheat and maize when the canopy was fully developed; the same pattern was observed with CWC. This is due to the use of multi-year climatological baselines in ESI, which establish historical evaporative stress profiles, enabling reliable anomaly detection and maintaining efficiency even in the high seasonal variability. However, the well-characterized seasonal ET cycle may not always fully reflect recent shifts in climate variability or crop management practices. But it can minimize sensitivity to seasonal dynamics and mitigate the effects of cloud-induced data gaps. The biophysical variables are also sensitive to seasonal dynamics, and using long-term baselines is also recommended to mitigate the effects of cloud-induced data gaps or other sources of missing observations. Model-based approaches are generally more aligned with ground stations and are better than single-input variable-based drought indices (PDSI, SPEI, SPI) (Schmidt et al., 2024). For this reason, ESI and biophysical variables can be a reliable data choice for our study, with a track record of their performance linked to crop production anomalies.

One shortcoming is, ESI assumes a universal ET-PET response, which can limit its applicability in certain ecosystems. Like species- or ecosystem-specific responses, and the differences between isohydric and anisohydric species (which regulate water loss differently), can lead to varying interpretations of drought severity by ESI. As seen with rain-fed maize, ESI struggled to capture the full extent of the drought. At 4 km spatial resolution, it cannot fully capture spatial variability introduced by mixed irrigation practices, crop dynamics, and complex terrain, which can delay its detection in the drier regions where surface and subsurface soil moisture may be weakly coupled to ESI signals (Zhong et al., 2020).

The challenges in defining and classifying drought severity can further complicate the detection of flash droughts by variables. In the future, region-specific calibration, crop phenology, and yield data integrations would be useful for flash drought monitoring. Our study acknowledges, a single metric, either ESI or CWC, cannot adequately capture drought's multi-impact character in all its complexity, and CWC's rapid response can complement flash drought detection, especially in the irrigated cropping systems.

6. Conclusion

This study investigated the ability of SL2P-derived biophysical variables to monitor flash drought in irrigated and rainfed systems. The time series and temporal correlation analysis revealed that CWC has a strong agreement with ESI in the case of flash drought in the irrigated regions. It has the advantage of providing short-term and traceable information on crop response to drought events. The onset of flash drought can be detected with CWC, even amid crop development, because CWC is sensitive to rapid changes in moisture conditions. Our findings highlighted the importance of incorporating CWC into proactive drought monitoring systems, as early information on CWC at drought onset can assist in optimizing irrigation practices, diversifying crop portfolios, and adopting drought-tolerant varieties. Based on our results, CWC can be used as an early warning indicator for flash drought. However, these results can be further verified like CWC data derived from other estimators, i.e., hybrid physical models or ground-based observations.

CRediT authorship contribution statement

Zaib Unnisa: Writing – original draft, Validation, Methodology, Investigation, Formal analysis, Data curation, Conceptualization. **Booker Ogutu:** Writing – review & editing, Validation, Methodology, Investigation, Formal analysis. **Jadunandan Dash:** Writing – review & editing, Visualization, Supervision, Methodology, Formal analysis, Data curation, Conceptualization.

Ethical statement

This work has not been submitted or published elsewhere.
No AI-Generated tools have been used in the creation of this manuscript.

Declaration of competing interest

The authors declare that they have no known competing financial interests or personal relationships that could have appeared to influence the work reported in this paper.

Acknowledgements

This research is conducted through the support of the EO4CerealStress project, monitoring crop response to multiple stressors (ESA

AO/1–11144/22/I-EF), funded by the European Space Agency (ESA) under Agricultural Science Precursors – EXPRO+ (Theme 3).

Appendix 1

GIMMS– Global Agricultural Monitoring Crop Calendars

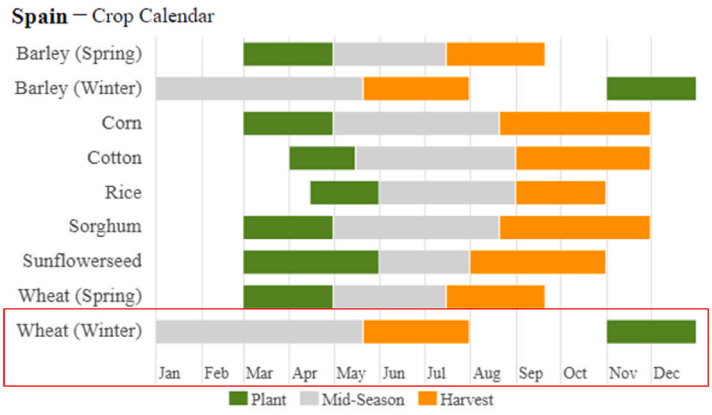

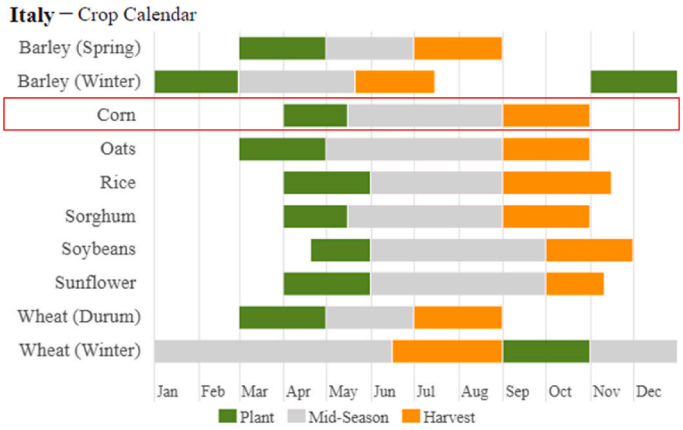

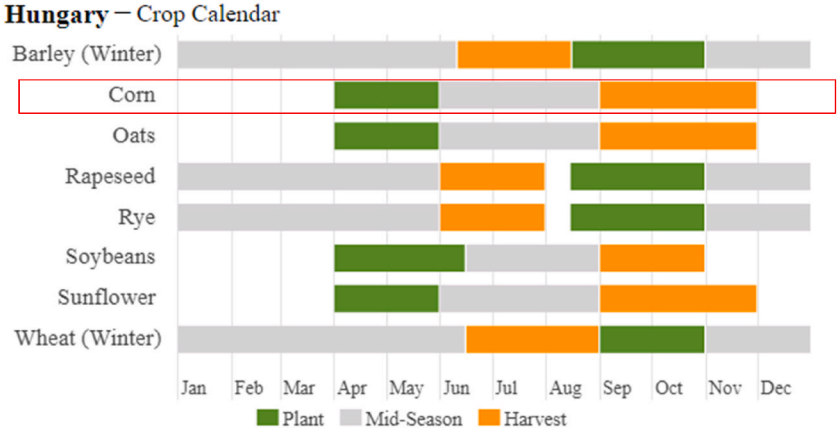

Appendix 2

ESI Threshold −2 results for ROI 1

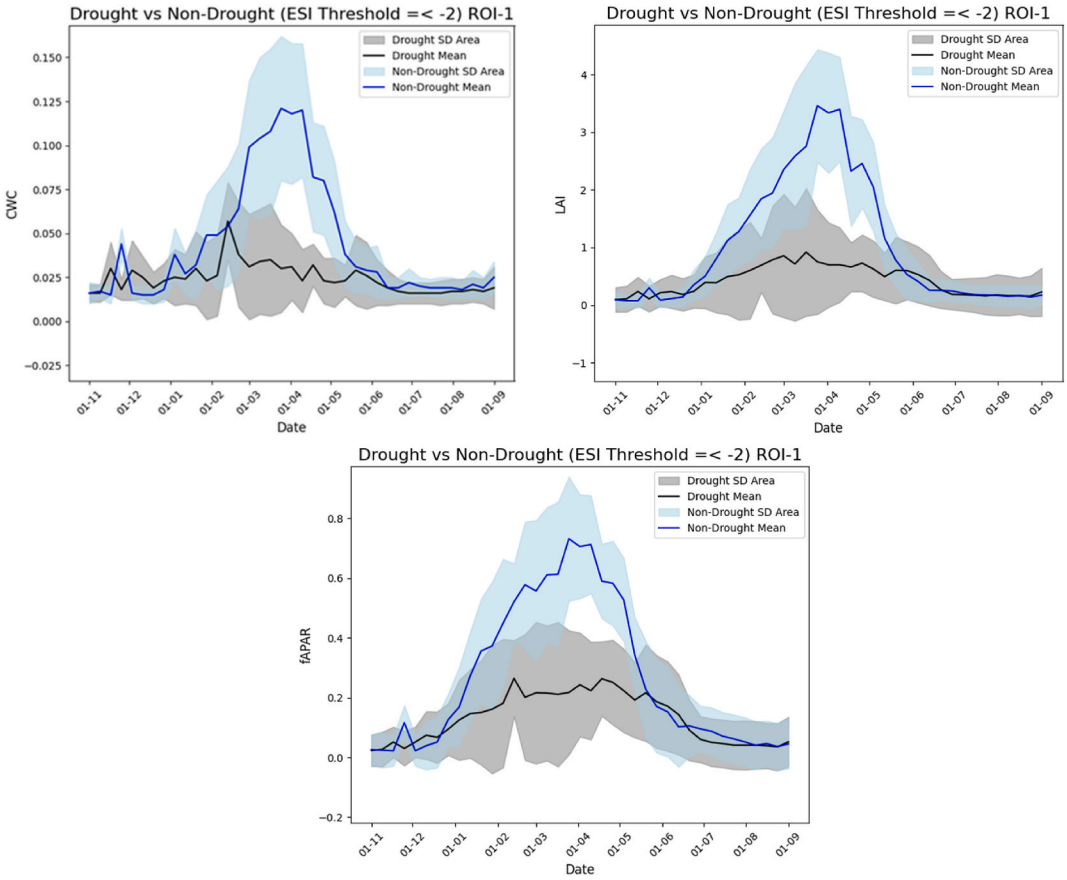

Fig. 9. Trends of ESI vs. CWC, LAI, and fAPAR mean and standard deviation during the wheat growing season for both drought (in grey) and non-drought (in blue) years with ESI -2 threshold

ESI Threshold −2 results for ROI 2 and ROI 3

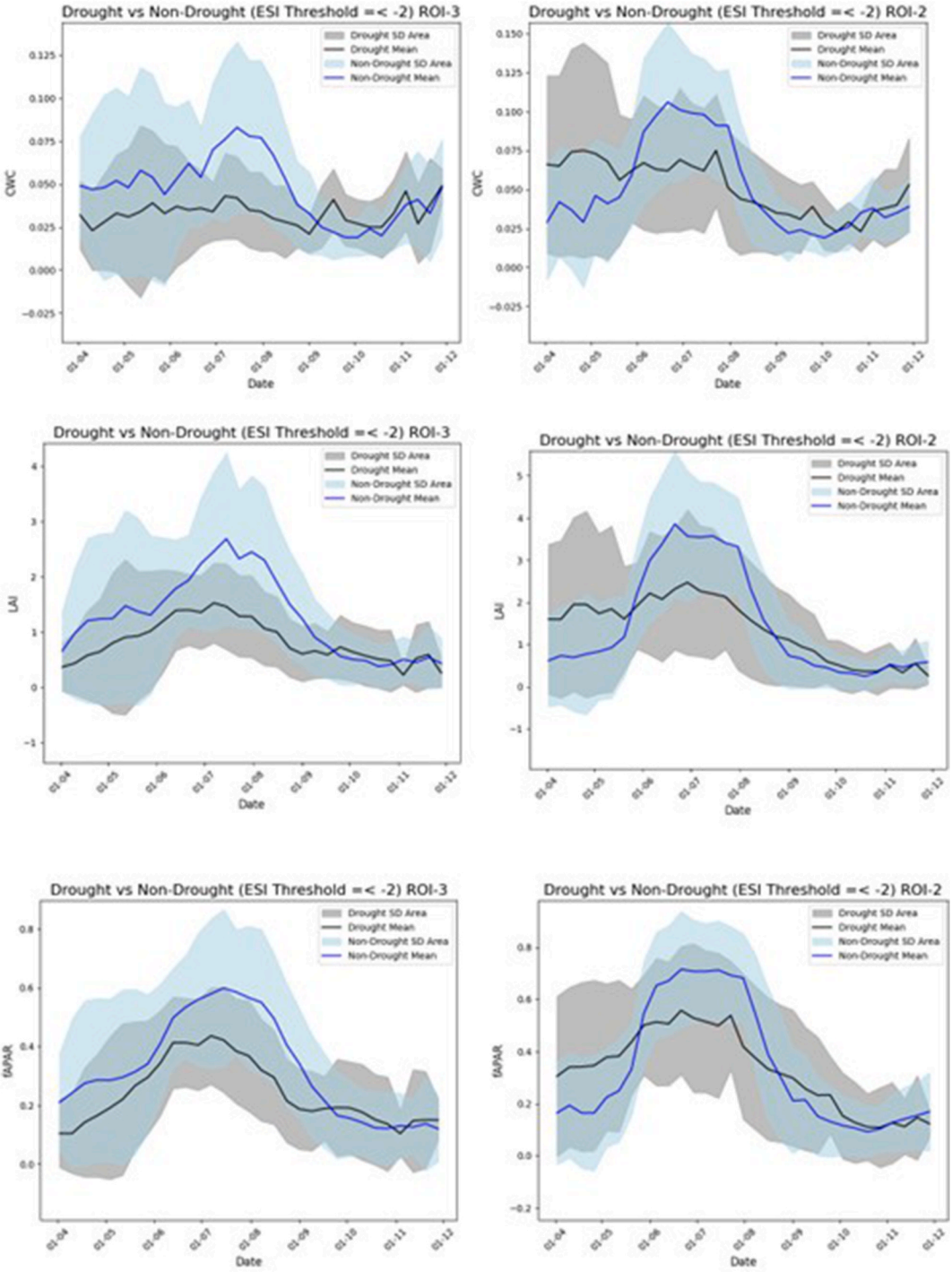

Fig. 10. Trends of ESI vs. CWC, LAI, and fAPAR mean and standard deviation during the maize growing season for both drought (in grey) and non-drought (in blue) years with ESI -2 threshold

Data availability

Data will be made available on request.

References

Ahmadi, F., Nazeri Tahroudi, M., Mirabbasi, R., Kumar, R., 2022. Spatiotemporal analysis of precipitation and temperature concentration using PCI and TCI: a case study of Khuzestan Province, Iran. Theor. Appl. Climatol. 149 (1), 743–760.

Alahacoon, N., Edirisinghe, M., 2022. A comprehensive assessment of remote sensing and traditional-based drought monitoring indices at global and regional scale. Geomat. Nat. Hazards Risk 13 (1), 762–799.

Allen, R.G., Pereira, L.S., Raes, D., Smith, M., 1998. Crop evapotranspiration-Guidelines for computing crop water requirements-FAO irrigation and drainage paper 56. Fao Rome 300 (9), D05109.

Anderson, M.C., Hain, C., Otkin, J., Zhan, X., Mo, K., Svoboda, M., Wardlow, B., Pimstein, A., 2013. An intercomparison of drought indicators based on thermal remote sensing and NLDAS-2 simulations with US drought monitor classifications. J. Hydrometeorol. 14 (4), 1035–1056.

Anderson, M.C., Zolin, C.A., Sentelhas, P.C., Hain, C.R., Semmens, K., Yilmaz, M.T., et al., 2016. The evaporative stress index as an indicator of agricultural drought in Brazil: an assessment based on crop yield impacts. Remote Sens. Environ. 174, 82–99. https://doi.org/10.1016/j.rse.2015.11.034.

Bachmair, S., Stahl, K., Collins, K., Hannaford, J., Acreman, M., Svoboda, M., Knutson, C., Smith, K.H., Wall, N., Fuchs, B., Crossman, N.D., 2016. Drought indicators revisited: the need for a wider consideration of environment and society. WIREs Water 3 (4), 516–536.

Baret, F., Weiss, M., Lacaze, R., Camacho, F., Makhmara, H., Pacholcyzk, P., Smets, B., 2013. GEOV1: LAI and FAPAR essential climate variables and FCOVER global time series capitalizing over existing products. Part1: principles of development and production. Remote Sens. Environ. 137, 299–309.

Barros, J.R.A., Guimarães, M.J.M., Simões, W.L., Melo, N.F.D., Angelotti, F., 2020. Water restriction in different phenological stages and increased temperature affect cowpea production. Cienc. E Agrotecnol 45, e022120.

Burka, A., Biazin, B., Bewket, W., 2024. Spatial drought occurrences and distribution using VCI, TCI, VHI, and Google Earth Engine in Bilate River Watershed, Rift valley of Ethiopia. Geomat. Nat. Hazards Risk 15 (1), 2377672.

Cammalleri, C., McCormick, N., Toreti, A., 2022. Analysis of the relationship between yield in cereals and remotely sensed fAPAR in the framework of monitoring drought impacts in Europe. Nat. Hazards Earth Syst. Sci. 22 (11), 3737–3750.

Chai, L., Jiang, H., Crow, W.T., Liu, S., Zhao, S., Liu, J., Yang, S., 2020. Estimating corn canopy water content from normalized difference water index (NDWI): an optimized NDWI-based scheme and its feasibility for retrieving corn VWC. IEEE Trans. Geosci. Remote Sens. 59 (10), 8168–8181.

Chang, Q., Ficklin, D.L., Jiao, W., Denham, S.O., Wood, J.D., Brunsell, N.A., et al., 2023. Earlier ecological drought detection by involving the interaction of phenology and Eco-physiological function. Earths Future 11 (3), e2022EF002667. https://doi.org/10.1029/2022EF002667.

Christian, J.I., Basara, J.B., Otkin, J.A., Hunt, E.D., Wakefield, R.A., Flanagan, P.X., Xiao, X., 2019. A methodology for flash drought identification: application of flash drought frequency across the United States. J. Hydrometeorol. 20 (5), 833–846.

Christian, J.I., Martin, E.R., Basara, J.B., Furtado, J.C., Otkin, J.A., Lowman, L.E., et al., 2023. Global projections of flash drought show increased risk in a warming climate. Commun. Earth Environ. 4 (1), 165.

Dao, P.D., He, Y., Proctor, C., 2021. Plant drought impact detection using ultra-high spatial resolution hyperspectral images and machine learning. Int. J. Appl. Earth Obs. Geoinf. 102, 102364. https://doi.org/10.1016/j.jag.2021.102364.

Djamai, N., Fernandes, R., Weiss, M., McNairn, H., Goïta, K., 2019. Validation of the Sentinel Simplified Level 2 Product Prototype Processor (SL2P) for mapping cropland biophysical variables using Sentinel-2/MSI and Landsat-8/OLI data. Remote Sens. Environ. 225, 416–430.

Du, L., Song, N., Liu, K., Hou, J., Hu, Y., Zhu, Y., et al., 2017. Comparison of two simulation methods of the temperature vegetation dryness index (TVDI) for drought monitoring in semi-arid regions of China. Remote Sens. 9 (2), 177.

Dutta, D., Kundu, A., Patel, N.R., Saha, S.K., Siddiqui, A.R., 2015. Assessment of agricultural drought in Rajasthan (India) using remote sensing derived Vegetation Condition Index (VCI) and Standardized Precipitation Index (SPI). Egypt. J. Remote Sens. Space Sci 18 (1), 53–63.

d'Andrimont, R., Verhegghen, A., Lemoine, G., Kempeneers, P., Meroni, M., Van Der Velde, M., 2021. From parcel to continental scale–A first European crop type map based on Sentinel-1 and LUCAS Copernicus in-situ observations. Remote Sens. Environ. 266, 112708. https://doi.org/10.1016/j.rse.2021.112708.

Eswar, R., Das, N.N., Poulsen, C., Behrangi, A., Swigart, J., Svoboda, M., et al., 2018. SMAP soil moisture change as an indicator of drought conditions. Remote Sens. 10 (5), 788. https://doi.org/10.3390/rs10050788.

Fernandes, R., Brown, L., Canisius, F., Dash, J., He, L., Hong, G., et al., 2023. Validation of Simplified Level 2 Prototype Processor Sentinel-2 fraction of canopy cover, fraction of absorbed photosynthetically active radiation and leaf area index products over North American forests. Remote Sens. Environ. 293, 113600. https://doi.org/10.1016/j.rse.2023.113600.

Food and Agriculture Organization of the United Nations (FAO), 2016. Agricultural Stress Index System (ASIS). FAO, Rome. Retrieved from. http://www.fao.org/giews/earthobservation.

Gao, S., Zhong, R., Yan, K., Ma, X., Chen, X., Pu, J., et al., 2023. Evaluating the saturation effect of vegetation indices in forests using 3D radiative transfer simulations and satellite observations. Remote Sens. Environ. 295, 113665. https://doi.org/10.1016/j.rse.2023.113665.

Genangeli, A., Avola, G., Bindi, M., Cantini, C., Cellini, F., Grillo, S., et al., 2023. Low-cost hyperspectral imaging to detect drought stress in high-throughput phenotyping. Plants 12 (8), 1730. https://doi.org/10.3390/plants12081730.

Guttman, N.B., 1998. Comparing the Palmer drought index and the standardized precipitation index 1. JAWRA J. Am. Water Resour. Assoc. 34 (1), 113–121.

Hansel, S., Hoy, A., Brendel, C., Maugeri, M., 2022. Record summers in Europe: variations in drought and heavy precipitation during 1901–2018. Int. J. Climatol. 42 (12), 6235–6257.

Hari, V., Rakovec, O., Markonis, Y., Hanel, M., Kumar, R., 2020. Increased future occurrences of the exceptional 2018–2019 Central European drought under global warming. Sci. Rep. 10 (1), 12207.

Hassanpour, R., Majnooni-Heris, A., Fakheri Fard, A., Verrelst, J., 2024. Monitoring biophysical variables (FVC, LAI, LCab, and CWC) and cropland dynamics at field scale using Sentinel-2 time series. Remote Sens. 16 (13), 2284. https://doi.org/10.3390/rs16132284.

Jacquemoud, S., Baret, F., 1990. PROSPECT: a model of leaf optical properties spectra. Remote Sens. Environ. 34 (2), 75–91. https://doi.org/10.1016/0034-4257(90)90100-Z.

Javed, T., Li, Y., Feng, K., Ayantobo, O.O., Ahmad, S., Chen, X., et al., 2021. Monitoring responses of vegetation phenology and productivity to extreme climatic conditions using remote sensing across different sub-regions of China. Environ. Sci. Pollut. Res. 28, 3644–3659.

Jiao, W., Zhang, L., Chang, Q., Fu, D., Cen, Y., Tong, Q., 2016. Evaluating an enhanced vegetation condition index (VCI) based on VIUPD for drought monitoring in the continental United States. Remote Sens. 8 (3), 224. https://doi.org/10.3390/rs8030224.

Kambona, C.M., Koua, P.A., Léon, J., Ballvora, A., 2023. Stress memory and its regulation in plants experiencing recurrent drought conditions. Theor. Appl. Genet. 136 (2), 26.

Kim, K., Wang, M.C., Ranjitkar, S., Liu, S.H., Xu, J.C., Zomer, R.J., 2017. Using leaf area index (LAI) to assess vegetation response to drought in Yunnan province of China. J. Mt. Sci. 14 (9), 1863–1872.

Lawal, S., Sitch, S., Lombardozzi, D., Nabel, J.E., Wey, H.W., Friedlingstein, P., et al., 2022. Investigating the response of leaf area index to droughts in southern African vegetation using observations and model simulations. Hydrol. Earth Syst. Sci. 26 (8), 2045–2071. https://doi.org/10.5194/hess-26-2045-2022.

Liu, S., Wu, Y., Xu, G., Cheng, S., Zhong, Y., Zhang, Y., 2023. Characterizing the 2022 extreme drought event over the Poyang Lake Basin using multiple satellite remote sensing observations and in situ data. Remote Sens. 15 (21), 5125. https://doi.org/10.3390/rs15215125.

Lyons, D.S., Dobrowski, S.Z., Holden, Z.A., Maneta, M.P., Sala, A., 2021. Soil moisture variation drives canopy water content dynamics across the western US. Remote Sens. Environ. 253, 112233. https://doi.org/10.1016/j.rse.2020.112233.

Ma, Z.C., Sun, P., Zhang, Q., Hu, Y.Q., Jiang, W., 2021. Characterization and evaluation of MODIS-derived crop water stress index (CWSI) for monitoring drought from 2001 to 2017 over Inner Mongolia. Sustainability 13 (2), 916.
Markonis, Y., Kumar, R., Hanel, M., Rakovec, O., Máca, P., AghaKouchak, A., 2021. The rise of compound warm-season droughts in Europe. Sci. Adv. 7 (6), eabb9668. https://doi.org/10.1126/sciadv.abb9668.
Martínez-Dalmau, J., Gutiérrez-Martín, C., Kahil, T., Berbel, J., 2023. Impact of alternative water policies for drought adaptation in the Guadalquivir Mediterranean river basin, southern Spain. J. Hydrol. Reg. Stud. 47, 101444. https://doi.org/10.1016/j.ejrh.2023.101444.
Mohammadi, K., Jiang, Y., Wang, G., 2022. Flash drought early warning based on the trajectory of solar-induced chlorophyll fluorescence. Proc. Natl. Acad. Sci. U. S. A. 119 (32), e2202767119. https://doi.org/10.1073/pnas.2202767119.
Mohammed, S., Alsafadi, K., Daher, H., Gombos, B., Mahmood, S., Harsányi, E., 2020. Precipitation pattern changes and response of vegetation to drought variability in eastern Hungary. Bull. Natl. Res. Cent. 44, 1–10.
Monteleone, B., Borzí, I., 2024. Drought in the Po valley: identification, impacts and strategies to manage the events. Water 16 (8), 1187. https://doi.org/10.3390/w16081187.
Naumann, G., Cammalleri, C., Mentaschi, L., Feyen, L., 2021. Increased economic drought impacts in Europe with anthropogenic warming. Nat. Clim. Chang. 11 (6), 485–491.
Nguyen, H., Wheeler, M.C., Otkin, J.A., Cowan, T., Frost, A., Stone, R., 2019. Using the evaporative stress index to monitor flash drought in Australia. Environ. Res. Lett. 14 (6), 064016. https://doi.org/10.1088/1748-9326/ab2103.
Palmer, W.C., 1965. Meteorological Drought, vol 30. U.S. Department of Commerce, Weather Bureau.
Pasqualotto, N., Delegido, J., Van Wittenberghe, S., Verrelst, J., Rivera, J.P., Moreno, J., 2018. Retrieval of canopy water content of different crop types with two new hyperspectral indices: water absorption area index and depth water index. Int. J. Appl. Earth Obs. Geoinf. 67, 69–78. https://doi.org/10.1016/j.jag.2018.01.002.
Pinke, Z., Ács, T., Kalicz, P., Kern, Z., Jambor, A., 2024. Hotspots in the EU-27 and economic consequences of the 2022 spring-summer drought. EuroChoices 23 (1), 28–33.
Qiao, M., Hong, C., Jiao, Y., Hou, S., Gao, H., 2024. Impacts of drought on photosynthesis in major food crops and the related mechanisms of plant responses to drought. Plants 13 (13), 1808. https://doi.org/10.3390/plants13131808.
Rakovec, O., Samaniego, L., Hari, V., Markonis, Y., Moravec, V., Thober, S., et al., 2022. The 2018–2020 multi-year drought sets a new benchmark in Europe. Earths Future 10 (3), e2021EF002394. https://doi.org/10.1029/2021EF002394.
Schmidt, T., Schrön, M., Li, Z., Francke, T., Zacharias, S., Hildebrandt, A., Peng, J., 2024. Comprehensive quality assessment of satellite-and model-based soil moisture products against the COSMOS network in Germany. Remote Sens. Environ. 301, 113930.
Sehgal, V., Gaur, N., Mohanty, B.P., 2021. Global flash drought monitoring using surface soil moisture. Water Resour. Res. 57 (9), e2021WR029901. https://doi.org/10.1029/2021WR029901.
Sepulcre-Canto, G., Horion, S.M.A.F., Singleton, A., Carrao, H., Vogt, J., 2012. Development of a combined drought indicator to detect agricultural drought in Europe. Nat. Hazards Earth Syst. Sci. 12 (11), 3519–3531. https://doi.org/10.5194/nhess-12-3519-2012.
Shahzaman, M., Zhu, W., Bilal, M., Habtemicheal, B.A., Mustafa, F., Arshad, M., et al., 2021. Remote sensing indices for spatial monitoring of agricultural drought in South Asian countries. Remote Sens. 13 (11), 2059. https://doi.org/10.3390/rs13112059.
Sungmin, O., Park, S.K., 2023. Flash drought drives rapid vegetation stress in arid regions in Europe. Environ. Res. Lett. 18 (1), 014028.
Verhoef, W., 1984. Light scattering by leaf layers with application to canopy reflectance modeling: the SAIL model. Remote Sens. Environ. 16 (2), 125–141.
Verrelst, J., Camps-Valls, G., Muñoz-Marí, J., Rivera, J.P., Veroustraete, F., Clevers, J.G., Moreno, J., 2015. Optical remote sensing and the retrieval of terrestrial vegetation bio-geophysical properties–A review. ISPRS J. Photogramm. Remote Sens. 108, 273–290.
Vicca, S., Balzarolo, M., Filella, I., Granier, A., Herbst, M., Knohl, A., Peñuelas, J., 2016. Remotely-sensed detection of effects of extreme droughts on gross primary production. Sci. Rep. 6 (1), 28269.
Vicente Serrano, S.M., El Kenawy, A.M., Zabalza-Martínez, J., Noguera, I., Peña-Angulo, D., Juez, C., Lorenzo-Lacruz, J., 2023. Influence of the interannual variability of meteorological drought on the cross-interactions of ecological and hydrological drought in the central Spanish pyrenees. Remote Sens. Appl. Soc. Environ. https://doi.org/10.21138/GF.816.
Vicente-Serrano, S.M., Beguería, S., López-Moreno, J.I., 2010. A multiscalar drought index sensitive to global warming: the standardized precipitation evapotranspiration index. J. Clim. 23 (7), 1696–1718.
Vicente-Serrano, S.M., Gouveia, C., Camarero, J.J., Beguería, S., Trigo, R., López-Moreno, J.I., Sanchez-Lorenzo, A., 2013. Response of vegetation to drought time-scales across global land biomes. Proc. Natl. Acad. Sci. 110 (1), 52–57.
Wei, W., Zhang, J., Zhou, L., Xie, B., Zhou, J., Li, C., 2021. Comparative evaluation of drought indices for monitoring drought based on remote sensing data. Environ. Sci. Pollut. Res. 28, 20408–20425.
Yihdego, Y., Vaheddoost, B., Al-Weshah, R.A., 2019. Drought Indices Indicators Revisited. Arabian J. Geosci. 12, 1–12.
Zargar, A., Sadiq, R., Naser, B., Khan, F.I., 2011. A review of drought indices. Environ. Rev. 19, 333–349.
Zeng, J., Zhang, R., Qu, Y., Bento, V.A., Zhou, T., Lin, Y., et al., 2022. Improving the drought monitoring capability of VHI at the global scale via ensemble indices for various vegetation types from 2001 to 2018. Weather Clim. Extrem. 35, 100412. https://doi.org/10.1016/j.wace.2022.100412.
Zhang, F., Zhou, G., 2019. Estimation of vegetation water content using hyperspectral vegetation indices: a comparison of crop water indicators in response to water stress treatments for summer maize. BMC Ecol. 19, 1–12.
Zhong, Y., Otkin, J.A., Anderson, M.C., Hain, C., 2020. Investigating the relationship between the evaporative stress index and land surface conditions in the contiguous United States. J. Hydrometeorol. 21 (7), 1469–1484.
Zhou, H., Zhou, G., He, Q., Zhou, L., Ji, Y., Lv, X., 2021. Capability of leaf water content and its threshold values in reflection of soil–plant water status in maize during prolonged drought. Ecol. Indic. 124, 107395.
Zhou, H., Zhou, G., Song, X., He, Q., 2022. Dynamic characteristics of canopy and vegetation water content during an entire maize growing season in relation to spectral-based indices. Remote Sens. 14 (3), 584.